The Astrophysical Journal, 862:146 (21pp), 2018 August 1 https://doi.org/10.3847/1538-4357/aaca3c

Gaia–ESO Survey: INTRIGOSS—A New Library of High-resolution Synthetic Spectra

Mariagrazia Franchini[1], Carlo Morossi[1], Paolo Di Marcantonio[1], Miguel Chavez[2], Gerry Gilmore[3], Sofia Randich[4], Ettore Flaccomio[5], Sergey E. Koposov[3,6], Andreas J. Korn[7], Amelia Bayo[8], Giovanni Carraro[9], Andy Casey[10], Elena Franciosini[4], Anna Hourihane[3], Paula Jofré[3,11], Carmela Lardo[12], James Lewis[3], Laura Magrini[4], Lorenzo Morbidelli[4], G. G. Sacco[4], Clare Worley[3], and Tomaz Zwitter[13]

[1] INAF—Osservatorio Astronomico di Trieste, Via G. B. Tiepolo 11, Trieste, I-34143, Italy; mariagrazia.franchini@inaf.it
[2] Instituto Nacional de Astrofísica, Óptica y Electrónica, Luis Enrique Erro 1, 72840 Tonantzintla, Puebla, Mexico
[3] Institute of Astronomy, University of Cambridge, Madingley Road, Cambridge CB3 0HA, UK
[4] INAF—Osservatorio Astrofisico di Arcetri, Largo E. Fermi 5, Florence, I-50125, Italy
[5] INAF—Osservatorio Astronomico di Palermo, Piazza del Parlamento 1, Palermo, I-90134, Italy
[6] McWilliams Center for Cosmology, Department of Physics, Carnegie Mellon University, 5000 Forbes Avenue, Pittsburgh, PA 15213, USA
[7] Department of Physics and Astronomy, Uppsala University, Box 516, SE-751 20 Uppsala, Sweden
[8] Instituto de Física y Astronomiía, Fac. de Ciencias, Universidad de Valparaíso, Gran Bretaña 1111, Playa Ancha, Chile
[9] Dipartimento di Fisica e Astronomia, Università di Padova, Vicolo dell'Osservatorio 3, Padova, I-35122, Italy
[10] Monash Centre for Astrophysics, School of Physics & Astronomy, Monash University, Clayton 3800, Victoria, Australia
[11] Núcleo de Astronomía, Facultad de Ingeniería, Universidad Diego Portales, Av. Ejército 441, Santiago, Chile
[12] Laboratoire d'astrophysique, Ecole Polytechnique Fédérale de Lausanne (EPFL), Observatoire de Sauverny, CH-1290 Versoix, Switzerland
[13] Faculty of Mathematics and Physics, University of Ljubljana, Jadranska 19, 1000, Ljubljana, Slovenia
Received 2018 February 6; revised 2018 June 1; accepted 2018 June 1; published 2018 August 1

Abstract

We present a high-resolution synthetic spectral library, INTRIGOSS, designed for studying FGK stars. The library is based on atmosphere models computed with specified individual element abundances via ATLAS12 code. Normalized SPectra (NSPs) and surface Flux SPectra (FSP) in the wavelength range 4830–5400 Å were computed with the SPECTRUM code. INTRIGOSS uses the solar composition of Grevesse et al. and four [α/Fe] abundance ratios, and consists of 15,232 spectra. The synthetic spectra are computed with astrophysical *gf*-values derived by comparing synthetic predictions with a solar spectrum of very high signal-to-noise ratio and the UVES-U580 spectra of five cool giants. The validity of the NSPs is assessed by using the UVES-U580 spectra of 2212 stars observed in the framework of the *Gaia*–ESO (European Southern Observatory) survey and characterized by homogeneous and accurate atmospheric parameter values and by detailed chemical compositions. The greater accuracy of NSPs with respect to spectra from the synthetic spectral libraries AMBRE, GES_Grid, PHOENIX, C14, and B17 is demonstrated by evaluating the consistency of the predictions of the different libraries for stars in the UVES-U580 sample. The validity of the FSPs is checked by comparing their prediction with both the observed spectral energy distribution (SED) and spectral indices. The comparison of FSPs with SEDs derived from the libraries ELODIE, INDO–U.S., and MILES indicates that the former reproduce the observed flux distributions within a few per cent and without any systematic trend. The good agreement between observational and synthetic Lick/SDSS (Sloan Digital Sky Survey) indices shows that the predicted blanketing of FSPs well reproduces the observed one, thus confirming the reliability of INTRIGOSS FSPs.

Key words: astronomical databases: miscellaneous – stars: late-type

1. Introduction

The use of stellar spectral libraries dates back several decades, with some of the most prominent examples being the data set constructed by Jacoby et al. (1984) and that of Kurucz (1979), which provide examples, respectively, of empirical and theoretical approaches to understanding stellar atmospheres, in particular the photospheres. Over the nearly 40 years since those papers a wealth of works have provided very extensive spectral libraries that have (partially) coped with the drawbacks found in the different approaches. On the empirical side, newer databases contain higher resolution spectra (e.g., ELODIE (Moultaka et al. 2004); Sloan Digital Sky Survey (SDSS) as, for example, SEGUE (Yanny et al. 2009) and APOGEE (Majewski et al. 2017); the Galactic Archaeology with HERMES (GALAH) survey (De Silva et al. 2015); *Gaia*–European Southern Observatory (ESO) survey (GES, Gilmore et al. 2012; Randich et al. 2013 etc.) with a much more comprehensive coverage of the parameter space (i.e., in effective temperature, $T_{\rm eff}$, surface gravity, log g, and chemical composition, [Fe/H] and [α/Fe]) and wavelength. On the theoretical side, current available libraries of theoretical spectra have incorporated more extended line lists and updated atomic and molecular parameters in addition to a more detailed calculation of the radiative transfer equation allowing for departures from local thermodynamic equilibrium, and in general including a more realistic treatment of the physical processes, e.g., motions, from microturbulence to 3D dynamics of convection, than those that characterize a classical model atmosphere (Hubeny 1988; Husser et al. 2013, etc.).

Stellar libraries have been extensively applied in a number of astrophysical topics such as:

1. automatic analysis of data in stellar surveys to derive atmospheric parameters, radial and rotational velocities;
2. detection of exoplanets via cross-correlation with spectral templates;
3. study of the star formation history of galaxies by using synthetic and observed photometric indices and/or spectral energy distributions (SEDs).

It is practically impossible to review here the full set of applications; however, the compilation of Leitherer et al. (1996) gives evidence of the use of spectroscopic stellar data sets in the particular case of, perhaps, the most widely spread implementation: studies of galaxy structure and evolution.

It is worthwhile noticing that most of the empirical libraries contain imprints of the local properties of the solar neighborhood, thus hampering the study of stellar populations characterized by a star formation history different from that in our vicinity. Therefore, several theoretical libraries were computed to complement the empirical ones and these are available in the literature (e.g., Coelho et al. 2005, C05; de Laverny et al. 2012, AMBRE; Husser et al. 2013, PHOENIX; Coelho 2014, C14; Brahm et al. 2017, B17). As mentioned before, these theoretical libraries can be used to derive stellar atmospheric parameters by comparing observed spectra with their predictions, even if some limitations arise from the approximation and inaccuracies in the models and input data used to compute them.

The computation of a theoretical library consists in the calculation of a set of model atmospheres giving the distributions of temperature, gas, electrons, and radiation pressure as a function of column mass or optical depth and the computation of the emerging spectra via a spectral synthesis code. Of the set of atmosphere models the most commonly used for the analysis of Sun-like stars are those computed with the codes ATLAS9 (Castelli & Kurucz 2003), ATLAS12 (Kurucz 2005a), MARCS (Gustafsson et al. 2008), or PHOENIX (Hauschildt & Baron 1999), while synthetic spectra may be computed with several spectral synthesis codes such as DFSYNTHE (Castelli 2005; Kurucz 2005a, 2005b), SPECTRUM (Gray & Corbally 1994), PHOENIX, MOOG,[14] etc.

The available libraries in the literature differ not only because of the different model and synthesis codes used but also because of different adopted chemical mixtures and different atomic and molecular line lists. Moreover, not all the libraries provide both normalized high-resolution (HR) spectra and SEDs since they require different approaches (see, for example, the discussion in C14).

A comparison of the performances of existing libraries is given in B17, where the authors presented their synthetic spectral library devoted to the determination of atmospheric stellar parameters via the Zonal Atmospheric Stellar Parameters Estimator (ZASPE). Even if the B17 spectral library is able to obtain results more consistent with the SWEET-Cat catalog used to validate ZASPE code than C05 and PHOENIX, such a library, adopting solar-scale abundances, may introduce systematic biases in the determination of $\log g$ values for stars having non-solar [Mg/Fe] (see B17). Furthermore, the B17 library consists only of normalized HR spectra and therefore is not fully suited for stellar population studies requiring SEDs.

In this paper we present a new library of HR synthetic spectra, INaf-TRIeste Grid Of Synthetic Spectra (INTRIGOSS), for F, G, K stars covering the wavelength range from 4830 to 5400 Å, which, though rather narrow, is very useful for deriving values of stellar atmospheric parameters for these stellar types. The INTRIGOSS spectral library, which is available on the web,[15] aims to provide a tool for determination of stellar atmospheric parameters and it consists of Normalized SPectra (NSPs) and surface Flux SPectra (FSPs). Model atmospheres and theoretical spectra were obtained assuming for the solar composition that derived by Grevesse et al. (2007), and the full consistency of the library was guaranteed by using the codes ATLAS12 and SPECTRUM v2.76f, which allowed us to specify the same individual element abundances in deriving both the structures of the atmospheres and the emerging spectra. The NSPs and FSPs were computed with an atomic and molecular line list built by tuning oscillator strengths in order to reproduce a set of HR reference spectra, namely the solar spectrum and the GES spectra of five cool giants with high signal-to-noise ratios ($S/N > 100$). The final line list includes also a subset of bona fide predicted lines (PLs). The PLs are calculated absorption lines corresponding to transitions between levels predicted by atomic structure codes but not measured in the laboratory, and they are affected by large uncertainties in their computed intensity and wavelength. We call bona fide PLs those with wavelength positions and oscillator strengths consistent with the features in the HR reference spectra and which can be safely used to compute reliable SEDs. The NSPs and FSPs are computed with a wavelength sampling of 0.01 Å, thus allowing their degradation at any resolving power $R \lesssim 240{,}000$.

INTRIGOSS covers the following ranges in the parameter space: $T_{\rm eff}$ from 3750 to 7000 K, $\log g$ from 0.5 to 5.0 dex, and [Fe/H] from −1.0 to +0.5 dex. Furthermore, to also account for stars with non-solar scaled abundances of α elements, four different chemical compositions were adopted: $[\alpha/{\rm Fe}] = -0.25$, 0.00, +0.25, and +0.50.

The validity of the line list used in computing INTRIGOSS NSPs and FSPs, and the improvement of INTRIGOSS NSPs over those of the already available libraries, is attested to by comparing them with a set of 2212 GES UVES spectra (hereafter UVES-U580 sample) obtained in a setup centered at 580 nm (UVES-580) in the framework of the iDR4 release of the *Gaia*–ESO survey. GES was designed to target all major Galactic components (i.e., bulge, thin and thick disks, halo, and clusters), with the goal of constraining the chemical and dynamical evolution of the Milky Way (Gilmore et al. 2012; Randich et al. 2013). When completed, the survey will have observed with Fibre Large Array Multi Element Spectrograph/UV–Visual Echelle Spectrograph (FLAMES/UVES) a sample of several thousand FGK-type stars within 2 kpc of the Sun in order to derive the detailed kinematic and elemental abundance distribution functions of the solar neighborhood. The sample includes mainly thin and thick disk stars, of all ages and metallicities, but also a small fraction of local halo stars. Data reduction of the FLAMES/UVES spectra has been performed using a workflow specifically developed for this project (Sacco et al. 2014). The iDR4 release contains radial and rotational velocities, recommended stellar atmospheric parameters, and individual element abundances. It also contains the stacked spectra derived from observations made for the *Gaia*–ESO survey during iDR4 and tables of metadata summarizing these spectra. The UVES-580 spectra were analyzed with the *Gaia*–ESO multiple pipelines strategy, as described in Smiljanic et al. (2014). The results of each pipeline are combined with an updated methodology (A. Casey et al. 2018, in preparation) to define the final set of recommended values of the atmospheric parameters and chemical abundances that are part of iDR4 (see also Magrini et al. 2017).

[14] http://www.as.utexas.edu/~chris/moog.html
[15] http://archives.ia2.inaf.it/intrigoss/

The validity of the INTRIGOSS FSPs is checked by comparing observed and synthetic SEDs for a subsample of stars and through the analysis of synthetic photometric indices computed for all the UVES-U580 stars from the corresponding derived FSPs. In particular, in this paper, we show the very good agreement between observational and INTRIGOSS synthetic Mg_1, Mg_2, and Mgb Lick/SDSS indices (Franchini et al. 2010).

In Section 2 we describe how the models and the synthetic spectra were computed, the atomic and molecular line lists we used, and the sample of UVES-U580 spectra adopted as reference to check the reliability of our library. Section 3 compares the predictions of INTRIGOSS with those of publicly available spectral libraries and discusses the improvements achieved. In Section 4 we describe the INTRIGOSS data products and auxiliary files available on the web. Finally, in Section 5 we summarize and conclude.

2. The Theoretical Library of Synthetic Spectra: INTRIGOSS

The construction of a theoretical stellar library requires several fundamental ingredients that are applied in different steps. The two main ingredients are (a) a set of model atmospheres that are needed as input in the calculation of synthetic spectra and (b) a fiducial line list to take into account the relevant individual atomic as well as molecular transitions expected to be important for the parameter space under consideration. Additionally, one requires the appropriate codes for the computations and the choice of the spectrum/spectra to which the theoretical data set will be compared to check the capability of the library in representing real stars.

The construction of INTRIGOSS consists of several steps. The first is the calculation of a grid of model atmospheres that provide the variation of physical quantities throughout the atmosphere. This task has been carried out by using the ATLAS12 code developed by Kurucz (2005a). Once a set of theoretical models has been constructed, the next step is to calculate, under the same considerations (i.e., local thermodynamic equilibrium, LTE), the corresponding synthetic spectra at high resolution. If the input fiducial atomic and molecular line list is adequate to predict line profiles of observed spectra, this would be the second and last step in the process; nevertheless, any working line list actually needs fine-tuning of the main agent that affects line intensities, i.e., the oscillator strengths or the $\log(gf)$ values, for the (at least) more prominent transitions. This last task is usually conducted by comparing synthetic spectra with observed data of the highest quality. Below we provide details of these processes that end up with the theoretical library INTRIGOSS.

2.1. The Atmosphere Models

As discussed in Kurucz (2005a) and Castelli (2005), ATLAS12 can generate an atmosphere model for any desired individual chemical composition of elements and microturbulent velocity (ξ), since the treatment of opacity is based on the opacity sampling technique, instead of the opacity distribution functions method used, for example, by ATLAS9. We adopted for the reference solar abundances those obtained from Grevesse et al. (2007), which have a wide consensus in the literature and whose validity is also confirmed, within the quoted uncertainties, by the abundance determinations derived by the Working Group 11 (WG11) of the *Gaia*–ESO consortium (Magrini et al. 2017) from the analysis of solar and M67 giant UVES spectra obtained with the U580 and U520 setups (Dekker et al. 2000).

We computed sets of atmosphere models in the following ranges of atmospheric parameters:

1. $T_{\rm eff}$ from 3750 to 7000 K in steps of 250 K;
2. $\log g$ from 0.5 to 5.0 dex in steps of 0.5 dex;
3. [Fe/H] from −1.0 to +0.5 dex in steps of 0.25 dex;
4. [α/Fe] from −0.25 to +0.5 dex in steps of 0.25 dex, where the α elements considered are O, Ne, Mg, Si, S, Ar, Ca, and Ti;
5. ξ equal to 1 and 2 km s^{-1}.

Our atmosphere models were calculated by using ATLAS12, and as initial starting models the ATLAS9 model atmospheres calculated for the APOGEE survey available online.[16] The resulting models computed with the two ξ values were checked by looking at the behaviors of temperature, gas pressure, electron density, Rosseland absorption coefficient, and radiation pressure at all Rosseland optical depths. The few gaps in the coverage of the resulting atmosphere models in the $T_{\rm eff}$–$\log g$ plane correspond to the absence of initial models in the APOGEE set. In running ATLAS12 we used in input atomic and molecular species (file *molecules.dat*[17]) the lines of all the elements in the first five stages of ionization (*fclowlines.bin*[18]), the lines of diatomic molecules (*diatomicsiwl.bin*[18] and *tioschwenke.bin*[19] by Schwenke 1998), and the lines of H_2O (*h2ofastfix.bin*[20]) by Partridge & Schwenke (1997). The adopted steps in $T_{\rm eff}$, $\log g$, [Fe/H], and [α/Fe] correspond roughly to twice the standard uncertainties in the determinations of atmospheric parameters quoted in the literature (see for example Magrini et al. 2017). It is worth noting that, on the basis of the considerations presented in Sections 3.1 and 3.2, a smaller step in temperature would make safer any interpolation required for deriving stellar atmospheric parameters. Therefore, in a future extended version of INTRIGOSS aimed at increasing, in particular, its wavelength coverage, we plan to adopt a finer temperature grid.

2.2. The Synthetic Spectra

To obtain from each atmosphere model the corresponding emergent flux and normalized spectrum we used SPECTRUM v2.76f. SPECTRUM is a stellar spectral synthesis program that calculates, under the LTE approximation, the synthetic spectrum for a given model atmosphere. The code additionally requires line lists of atomic and molecular transitions, which should be as accurate and complete as possible, and supports all expected atomic elements and the following diatomic molecules: H_2, CH, NH, OH, MgH, SiH, CaH, SiO, C_2, CN, CO, and TiO. The code can deliver both the stellar-disk-integrated normalized spectrum and the absolute monochromatic flux at the stellar surface. The user should specify the wavelength range and sampling, the value of microturbulence velocity (ξ), and the individual element abundances to be used. For this work we have built a line

[16] http://www.iac.es/proyecto/ATLAS-APOGEE/
[17] http://kurucz.harvard.edu/programs/atlas12/
[18] http://kurucz.harvard.edu/linelists/linescd/
[19] http://kurucz.harvard.edu/molecules/tio/
[20] http://kurucz.harvard.edu/molecules/h2o/

Table 1
Giant Stars used to Derive Astrophysical log(gf) values

Cname	$T_{\rm eff}$ (K)	$\sigma_{T_{\rm eff}}$ (K)	log g (dex)	$\sigma_{\log g}$ (dex)	[Fe/H] (dex)	$\sigma_{\rm [Fe/H]}$ (dex)	ξ (km s^{-1})	σ_{ξ} (km s^{-1})	$V_{\rm rad}$ (km s^{-1})	$\sigma_{V_{\rm rad}}$ (km s^{-1})	$v \sin i$ (km s^{-1})	$\sigma_{v \sin i}$ (km s^{-1})	S/N[a]
00241708–7206106	4510	117	2.10	0.23	−0.70	0.10	1.34	0.08	2.91	0.57	2.15	2.82	108
00251219–7208053	4513	114	2.04	0.23	−0.67	0.10	1.45	0.03	−34.30	0.57	2.12	2.61	105
00240054–7208550	4541	121	2.06	0.23	−0.71	0.09	1.40	0.07	−13.13	0.57	2.10	2.56	108
02561410–0029286	4834	117	2.75	0.21	−0.70	0.09	1.05	0.05	−68.65	0.57	2.39	2.85	113
03173493–0022132	4966	121	3.14	0.23	−0.63	0.10	1.03	0.07	−40.28	0.57	2.22	2.51	113

Notes. Atmospheric parameter values from the recommended parameters and abundances table in the GESiDR4Final catalog.
[a] From the UVES-U580 FITS file headers.

list by merging the line data used by Lobel (2011, hereafter LO11) and the cool5.iso.lst line list kindly provided to us by R. O. Gray (2011, private communication), complemented with molecular lines of CH, NH, MgH, SiH, C_2, CN, and TiO and with both atomic (in the three main expected stages of ionization) and molecular PLs from Kurucz's site. The number of lines included in our calculations for the wavelength interval 4830–5400 Å is 1427,628 including 16,531, 339,652, and 1071,445 transitions for atomic, molecular, and PL entries, respectively.

As indicated previously, accurate computation of astrophysical synthetic spectra requires reliable atomic and molecular data, in particular accurate oscillator strengths, i.e., gf-values, for the transitions expected in the wavelength interval of interest. In recent years a number of online databases (i.e., NIST,[21] VALD,[22] NORAD,[23] the Kurucz website, etc.) have provided line data from a large variety of sources in the scientific literature. The gf-values given in the databases may either have been determined in the laboratory or derived from theoretical calculations. Thus the accuracy of these gf-values may vary widely from line to line; some are known with accuracies of 1% or better, while others may be off by orders of magnitude. A possible way to reduce these uncertainties is to compare high S/N spectra of stars, with well known atmospheric parameters and abundances, with their corresponding computed synthetic spectra. In this way the gf-values may be checked (and, if needed, adapted with a trial-and-error strategy) by looking for the best agreement between the synthetic and observed line profiles, thus deriving astrophysical gf-values. Since the line profiles depend both on stellar characteristics, namely $T_{\rm eff}$, log g, element abundance, and ξ, and on the gf-value, the risk in such an approach is to wrongly adapt the gf-values to compensate for potential inaccuracies in the assumed values of atmospheric parameters and in the modeling assumptions. It is therefore important to compare the synthetic and observed profiles of the same line in spectra of as many (and as different) stars as possible in order to disentangle the effect of incorrect gf-values from effects due to uncertainties in the other parameters.

In this context, LO11 used the high-resolution spectrum of three main-sequence stars, the Sun, Procyon, and ϵ Eri, characterized by the following $T_{\rm eff}$ (K), log g (dex), and ξ (km s^{-1}) values: Sun (5777, 4.438, 1.1), Procyon (6550, 4.0, 1.2), and ϵ Eri (5050, 4.5, 0.55), and assuming solar composition from Anders & Grevesse (1989) also for the last two stars. LO11 used the solar spectrum observed in 1981 with the NSO/KPNO Fourier transform spectrograph, degraded at $R \sim 80{,}000$, and, for Procyon and ϵ Eri, several optical spectra taken with the Hermes spectrometer on the 1.2 m Mercator telescope at La Palma Observatory, Canary Islands. The comparison synthetic spectra were calculated with the LTE radiative transfer code SCANSPEC[24], and in such a way LO11 updated the log(gf) values of 911 neutral lines in the wavelength range 4000–6800 Å. The main causes of uncertainties in the LO11 results arise from: (i) the problems of deriving the solar intensity (averaged over the solar disk) from the NSO/KPNO Fourier transform observations; (ii) the assumption of solar composition for Procyon and ϵ Eri, even if some differences in individual element abundances are reported in the literature (see for example Jofré et al. 2015); (iii) the use of only relatively high-temperature ($T_{\rm eff} > 5000$ K) main-sequence stars, which does not allow one to check the log(gf) values of those atomic and molecular lines that are mainly prominent in giants and/or cooler stars.

We decided to complement the work of LO11 by performing the same kind of analysis but by using a high S/N solar spectrum derived ad hoc and the UVES-U580 spectra with S/N above 100 of five giant stars (see Table 1) with atmospheric parameters in the following ranges: $T_{\rm eff}$ between 4500 and 5000 K, log g from 2.0 to 3.2 dex, and ξ from 1.0 to 1.5 km s^{-1}, and, for each star, the individual element abundances derived by GES Consortium and reported in the GESiDR4Final catalog (Magrini et al. 2017).

The outline of our method is the following:

1. use of the solar spectrum as the main reference to derive the astrophysical log(gf) values for atomic and molecular lines that are important at solar effective temperature and gravity by assuming no uncertainties in the solar parameters or in the adopted atmosphere model;
2. use of the five giant spectra to derive the astrophysical log (gf) values of those lines that are more prominent at temperatures and gravities lower than the solar ones and to fix globally the MgH opacity by using the scaling factor $f_{\rm MgH}$ (see Section 2.2.2);
3. use of a large sample of stars (more than 2200) covering a wider range of atmospheric parameter values to validate the final list of astrophysical log(gf) values.

[21] https://physics.nist.gov/PhysRefData/ASD/lines_form.html
[22] http://vald.astro.univie.ac.at/~vald3/php/vald.php
[23] http://www.pa.uky.edu/~peter/newpage/
[24] alobel.freeshell.org/scan.html

2.2.1. Refinement of Oscillator Strengths and Tuning of the Central Wavelengths: the Solar Case

We used an observed solar spectrum that is the average of 59 integrated sunlight spectra, as reflected by the Moon, taken with HARPS spectrograph at the 3.6 m La Silla ESO telescope. These spectra are the out-of-transit subsample of those taken to detect the Rossiter–McLaughlin effect in the Sun due to the Venus transit of 2012 June 6 (Molaro et al. 2013). The S/N of the average spectrum, as evaluated by looking at the ratio between the mean flux and the standard deviation of the mean at each wavelength, is about 4000. Then the spectrum was degraded at the resolution of the Hermes spectra ($R = 80{,}000$).

The normalized synthetic solar spectrum to be used in the comparison was computed with SPECTRUM starting from the ATLAS12 model obtained with $T_{\rm eff} = 5777$ K, $\log g = 4.4377$ dex, $\xi = 1.0$ km s^{-1}, and with the solar abundances of Grevesse et al. (2007). This spectrum was then degraded at $R = 80{,}000$ and convolved with the geometric mean of the solar $v \sin i$ and macroturbulence velocity values (2.5 km s^{-1}).

Prior to conducting modifications on the line data we first need to normalize the observed spectra, a crucial process to derive reliable log(gf)s. With the goal of matching the continuum levels of observed and synthetic spectra, we searched for continuum flux reference points in the normalized synthetic spectrum and identified the wavelength intervals with flux levels in excess of 0.99, avoiding, in this way, regions with absorption lines where the uncertainties in the log(gf) values may play a role. Then, the observed spectrum in each of the corresponding wavelength regions is divided by the synthetic one and these ratios are fitted with a polynomial. Eventually, the observed spectrum is divided by the polynomial so computed to obtain the normalized spectrum.

A trial-and-error procedure based on the comparison between the normalized and the synthetic solar spectra is now applied to modify (when needed) the input log(gf) values and/or the central wavelengths in order to match the profile of the observed lines or blends. We compared our observed and synthetic solar spectra to adapt the log(gf)s of those lines that are responsible for clearly detectable flux minima in the observed and/or synthetic spectra to obtain their astrophysical values. We followed a three-step approach:

1. we looked in our input line list to identify the transitions responsible for those minima present in both the observed and synthetic spectra and we iteratively modified their log (gf) values until we found a satisfactory agreement. In general we stopped the iteration when the difference between synthetic and observed spectra was below ± 0.003;
2. we selected the minima present only in the synthetic spectra and reduced the log(gf) values of the corresponding theoretical lines to match the observed spectrum;
3. we searched in our input line list and in the online databases listed in Section 2.2 for theoretical lines that may correspond to minima present only in the observed spectrum; for those lines found, we fine-tuned their log (gf) values and added them to our input list if needed.

In all the steps listed above we also checked the central wavelength of each identified feature, and in a few cases we slightly modified it to better match the observed spectrum. Eventually, the identification of the lines corresponding to the minima was double-checked by looking at the same wavelength regions in the synthetic and observed spectra of five giants (see Section 2.2.2).

In conclusion we derived astrophysical log(gf) values for 2229 lines, which include 850, 35, and 1344 atomic, molecular, and predicted transitions, respectively. The 850 atomic lines include 100 lines from LO11 that required slight modification of their log(gf) or of their central wavelength to get a better match to the spectra. These corrections are mainly due to the slightly different solar abundances adopted, to the higher S/N of our solar spectrum, and to the inclusion in our synthetic spectrum of molecular and predicted lines absent from the SCANSPEC spectra of LO11.

2.2.2. Refinement of Oscillator Strengths: Five Giant Stars

The above procedure should, in principle, be sufficient to calculate fiducial theoretical spectra that represent stars with atmospheric parameters close to solar. However, to account for potential targets of lower temperature and surface gravity one needs to extend the log(gf) tuning analysis to giant stars. For this extension we considered the five giants in Table 1.

We computed for each star i its synthetic spectrum (S_i) by using the GES atmospheric parameter values, the individual element abundances, and the line list that includes the astrophysical log(gf)s derived from the solar spectrum analysis. Then, we adopted the same procedures used for normalizing the observed solar spectrum for each giant i to derive from its UVES-580 spectrum the normalized one (O_i). First of all we checked that the modified log(gf) values obtained in Section 2.2.1 provide a good agreement of synthetic and observed spectra also for these five stars. We adopted a value of ± 0.01 as an acceptance threshold, which is larger than that used for the Sun due to the lower resolution ($R = 47{,}700$) and S/N ($\sim$100). Actually, in all but a very few cases, we did not need to go back to the analysis of the solar spectra to retune the log(gf)s. Then, we looked for features that were present only in the spectra of the giants. By adopting the same trial-and-error strategy used for the solar case but the new acceptance threshold we were able to derive astrophysical log(gf) values for an additional 175 lines, namely 49, 42, and 84 atomic, molecular, and predicted transitions, respectively. As far as the large number of weak lines of MgH, which is the dominant contributor to molecular opacity in our wavelength range, are concerned, we decided to check individually, for this molecule, only the log(gf)s of the strongest features. The contribution of the other MgH lines was then fine-tuned by means of a scaling factor, $f_{\rm MgH}$, by which their gfs are multiplied (see SPECTRUM documentation). To evaluate the most appropriate value of $f_{\rm MgH}$ we computed the Lick/SDSS Mg_1 and Mg_2 indices (Franchini et al. 2010), which are strongly affected by the MgH lines, from the UVES-U580 spectra and compared them with those from synthetic spectra calculated with $f_{\rm MgH}$ in the range 1.0–0.4. Figure 1 shows that, on the average, the best agreement is obtained with $f_{\rm MgH} = 0.45$.

It is important to remark that, should we consider that the need for such a low $f_{\rm MgH}$ is ascribed to uncertainties in the Mg abundances, one would require to decrease the Mg abundances, log(Mg/H), of all the five giants by $\sim$0.35 dex in order to keep the $f_{\rm MgH}$ value at 1.0. On the other hand, such low Mg abundances are inconsistent with those derived from the analysis of atomic Mg lines. Therefore, we are confident that the obtained $f_{\rm MgH} = 0.45$ is not due to a wrong GES

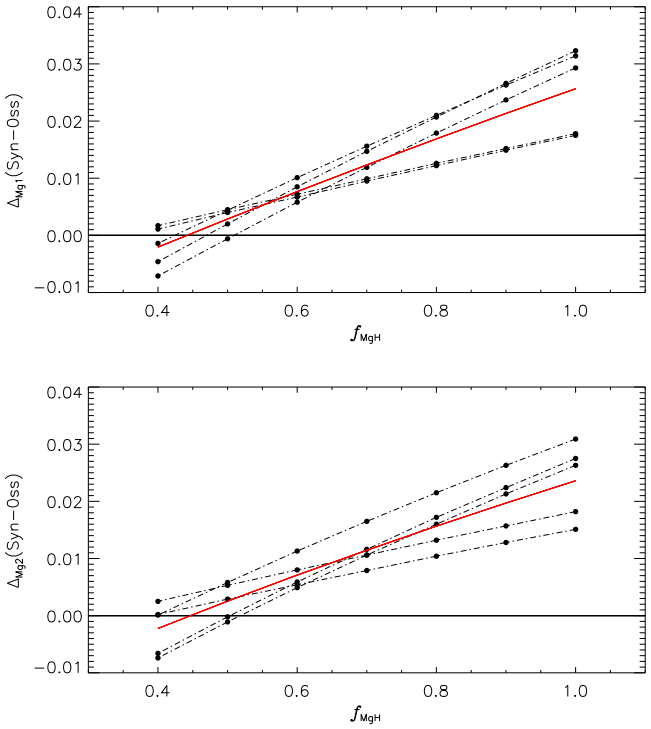

Figure 1. Differences between synthetic and observed Mg_1 and Mg_2 Lick/SDSS indices for the five giant stars in Table 1 (black dotted–dashed thin lines) and their average values (red thick line) as a function of the f_{MgH} value used in computing the synthetic spectra (see the text).

determination of magnesium abundance but to an overestimate of the MgH opacities computed by Kurucz (2014), as also found and discussed by Weck et al. (2003). Thus, hereafter we adopted the value $f_{MgH} = 0.45$ to correct such an overestimate and to be consistent with the log(Mg/H) derived from atomic lines.

2.3. Assessment of the Quality of the Modified Line List

Figures 2 and 3 show an example of the agreement between observed and synthetic spectra achieved by using the above-derived astrophysical log(*gf*)s. For the solar case, in which the uncertainties of the observed spectrum are negligible, a quantitative estimate of the improvement with respect to the use of the initial log(*gf*) list is given by the decrease in the standard deviation of the residuals from ∼0.06 to ∼0.03. In the case of the five giants, where observational uncertainties must be taken into account, we calculated, as a figure of merit, $r^i_{\rm med} = \mathrm{median}\left[\left(\frac{O_i(\lambda) - S_i(\lambda)}{\Delta O_i(\lambda)}\right)^2\right]$, where $\Delta O_i(\lambda)$ were obtained from the inverse variance-per-pixel given in the UVES-U580 FITS files. In computing $r^i_{\rm med}$ we excluded those wavelength regions that were used to normalize O_i because they are bound to near-zero residuals and are not sensitive to the quality of the log(*gf*)s used. We decided to use the median of the normalized residuals instead of the mean because the latter is strongly affected by the residuals in the region of unidentified lines. As can be seen in Table 2 the use of the astrophysical log(*gf*)s allows us to achieve a 30% decrease in the $r_{\rm med}$ values with respect to the initial ones.

We want to point out that some discrepancies still persist, in limited narrow wavelength regions, due to the presence in the observed spectra of lines that we were not able to find in any of the atomic and molecular databases available in the literature; being unidentified, they thus cannot be present in the synthetic spectra. A clear example of this situation is the feature at 5170.77 Å that is present in all observed spectra (see Figures 2, 3, and Table 4), and is particularly prominent in the solar one. We list the unidentified observed features in the Appendix.

2.4. Validation of Line List Improvements on the GES Sample

To check the validity of our line list, and consequently that of the synthesized spectra over the full atmospheric parameter space covered by F, G, and K stars, we decided to use a large sample of stars with well known atmospheric parameter values and individual element abundances. In what follows, we will use the observed spectra of 2212 UVES-U580 stars extracted from the fourth *Gaia*–ESO (iDR4) release, whose atmospheric parameter coverage is shown in Figure 4, in order to compare them with the corresponding individual synthetic NSPs. Our check is based on the important remark that, if we had derived wrong *gf*-values from the spectra of the Sun and of the five stars in Table 1 because of errors in the adopted stellar atmospheric parameters, these *gf*-values should be very ineffective in reproducing the observed spectra of stars covering a much more extended parameter space. Furthermore, we have to point out that any coupling between our astrophysical *gf*-values and GES determinations of atmospheric parameters is very unlikely since our main reference star in deriving astrophysical *gf*-values is the Sun (whose adopted atmospheric parameter values were not from GES). Moreover, the GES atmospheric parameter values of the five giants in Table 1 are the homogenized results of several Working Groups and Nodes of the *Gaia*–ESO consortium and are not at all related to the process conducted in this work for calculating theoretical models and spectra.

A first sample of 2616 stars was obtained by performing an SQL search to select all the stars in the effective temperature range 3500–7000 K and surface gravity range 0.25–5.25 dex observed with the U580 setup and characterized by an S/N greater than 10. Then, we removed all the stars with some peculiarity flag and/or lack of an error estimate of the stellar atmospheric parameters. In such a way we obtained a sample of 2311 stars that is suitable for our analysis since it contains objects with homogeneously determined $T_{\rm eff}$, $\log g$, detailed chemical composition, ξ, and $v \sin i$ spanning the following ranges: $T_{\rm eff}$ from 3900 to 7000 K, $\log g$ from 0.4 to 4.9 dex, [Fe/H] from −2.9 to +0.6 dex, [α/Fe] from −0.1 to +0.6 dex, and $\xi = 0.1$–$3.0\ \mathrm{km\ s^{-1}}$. For each star i we run ATLAS12 and SPECTRUM codes, using its GES atmospheric parameter values, individual element abundances (for those elements with no estimate of [X/Fe] we assumed [X/Fe] = 0), and our modified line list, to compute the appropriate normalized synthetic spectrum (S_i), which is then used to obtain a normalized one (O_i) from the corresponding observed (stacked) UVES-U580 spectrum. The normalization was performed by applying the same technique as for the solar spectrum. In few cases the S_i turned out to be significantly different from the O_i, in particular below 5167 Å. This region includes the C_2 bands of the Swan system (Swan 1857), and in particular the one used by Gonneau et al. (2016, Table 2) to define the C2U index, thus suggesting that the mismatch between S_i and O_i may be related to differences in the estimated and actual stellar carbon content. The determination of the abundance of C is quite challenging and the values of [C/Fe] derived by GES are, in general, less

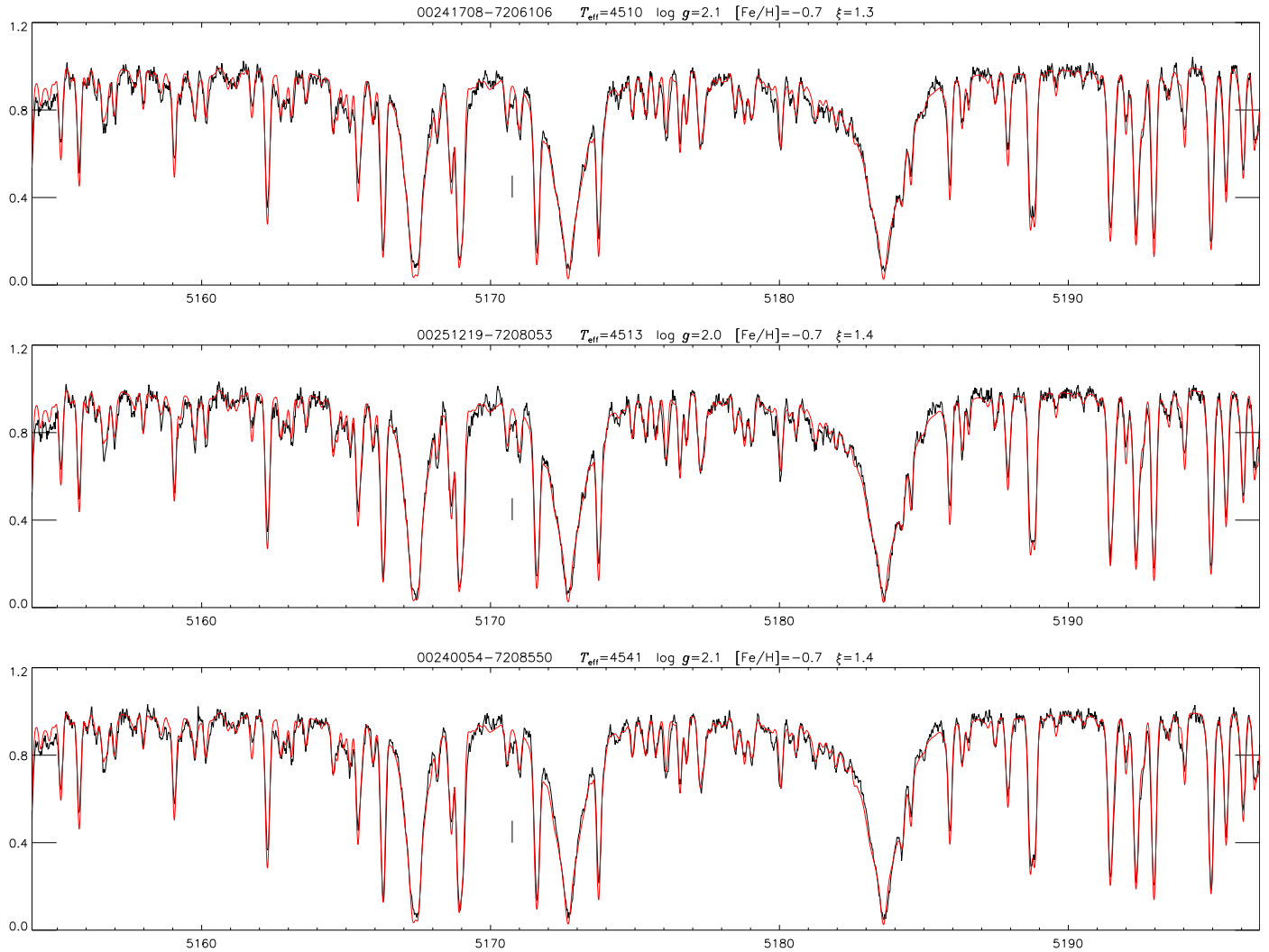

Figure 2. Example of the comparison between the observed spectra (black lines) and the synthetic ones (red lines) computed by using the derived astrophysical log (gf) for the first three giant stars in Table 1. As an example of unidentified lines the feature at 5170.77 Å is indicated (vertical bar).

accurate than for the other elements. In particular, GES does not include carbon abundances for 254 stars, and in almost all the other 2057 cases the estimated [C/Fe] is based on the analysis of only two spectral lines (1572 stars) or even just one (478 stars). To further investigate the role of [C/Fe] in the comparison of our synthetic spectra with the observed ones we computed the C2U index from both S_i and O_i for the whole sample of UVES-U580 stars. Figure 5 shows that, while in most cases the observed and synthetic C2U indices agree to within ± 0.05 mag, there are 99 stars that show larger differences, suggesting that their estimated (or assumed) [C/Fe] values are not correct. As a consequence, these stars are, for precaution, removed from our UVES-U580 sample, which in the end consists of 2212 stars with normalized observed spectra and NSPs.

In order to quantitatively estimate the agreement between each pair of S_i and O_i within the working GES sample, we calculate the same figure of merit, $r^i_{\rm med}$, used to compare the O_i and S_i spectra of the five giants in Table 1. The use of $r^i_{\rm med}$ as an estimate of the accuracy of our synthetic spectra requires, however, that we take into account that its value also depends on the uncertainties in the GES atmospheric parameters and in the normalization procedure. In order to investigate these two contributions we computed for each star, in addition to the figure of merit derived from synthetic spectra for the *nominal* set of GES atmospheric parameters and elemental abundances (which we call $n\_r^i_{\rm med}$), the synthetic spectra and the figure of merit by adding or subtracting for each atmospheric parameter the given 1σ uncertainty. Note that we have also obtained for each new S_i the corresponding normalized observed spectrum O_i.

The goodness of the GES estimates is confirmed by the general increase in $r^i_{\rm med}$ values with respect to the *nominal* ones when the S_i are computed considering the parameter uncertainties. We found that the main mean increase is caused by the adoption of $T_{\rm eff}-\sigma_{T\rm eff}$ and amounts to about 10%. The effects of varying the other parameters and of the normalization procedure turned out to be negligible.

The resulting distribution of the $n\_r^i_{\rm med}$ is presented in the top panel of Figure 6, which shows that the reliability of the astrophysical gf-values in our list, and therefore of the resulting synthetic spectra, is validated by the small $n\_r^i_{\rm med}$ values for the bulk of the 2212 stars. In fact, as can be seen, the $n\_r_{\rm med}$ distribution is strongly peaked at values below 1, with the maximum of the distribution between 0.6 and 0.7, attesting to the fact that, in most cases, the differences between S_i and O_i

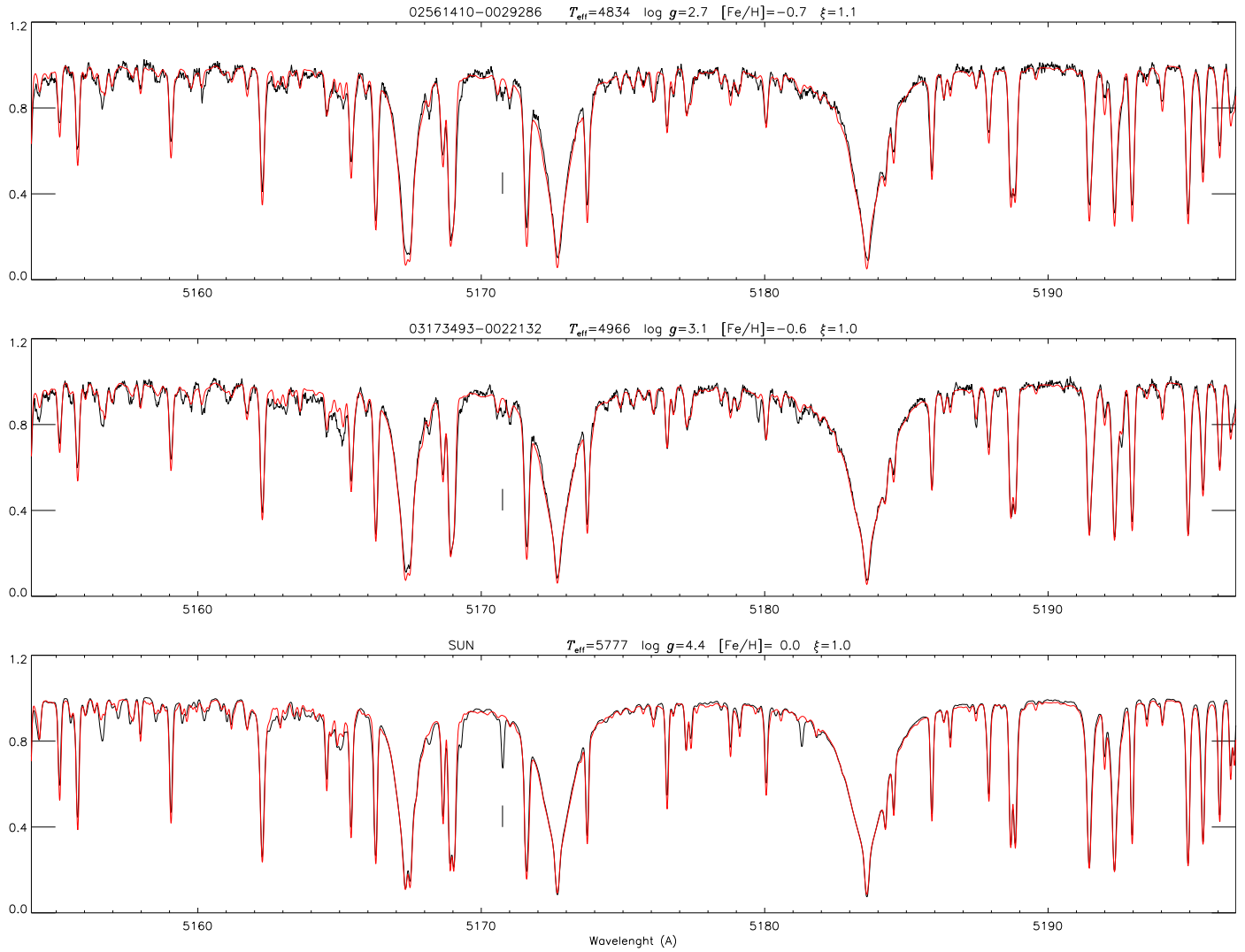

Figure 3. Example of the comparison between the observed spectra (black lines) and the synthetic ones (red lines) computed by using the derived astrophysical log (gf) for the last two giant stars in Table 1 and for the Sun. As an example of unidentified lines the feature at 5170.77 Å is indicated (vertical bar).

Table 2
Comparison of $r_{\rm med}$ Values for the Five Giants in Table 1 when Using Initial or Astrophysical log(gf)s

Cname	$r_{\rm med}$ Astrophysical	$r_{\rm med}$ Initial	Ratio (%)
00240054–7208550	1.46	2.10	69
00241708–7206106	1.30	1.84	71
02561410–0029286	1.33	1.96	68
00251219–7208053	0.89	1.37	65
03173493–0022132	0.76	1.14	67

are of the same order as (or even lower than) the estimated observational errors. The presence of a wing in the distribution toward higher $n\_r_{\rm med}$ values is mainly due, as expected, to the coolest stars, as can be seen in the second panel of Figure 6 where the median values of $n\_r^i_{\rm med}$ in partially overlapping bins containing 51 stars each ($\tilde{r}_{\rm med}$) are plotted versus $T_{\rm eff}$. Actually, for these objects, a lower accuracy of our synthetic spectra in reproducing the observed ones is somehow unavoidable due to both the difficulties in computing their atmosphere models and the absence, in our computations, of the triatomic molecular lines. In the third and fourth panels we depict the trends of $\tilde{r}_{\rm med}$ versus $\log g$ and [Fe/H], respectively. The increase in $\tilde{r}_{\rm med}$ for $\log g$ between 2.0 and 2.4 dex probably reflects the high number of cool GES stars in this gravity interval. The increase in $\tilde{r}_{\rm med}$ at [Fe/H] $\gtrsim 0$ can plausibly be attributed to the insufficient improvement (or lack of it) in the log(gf)s of weak lines in the solar and giant stellar spectra that are more prominent in the super-metal-rich regime.

In conclusion, we derived and validated astrophysical gf-values for 899, 77, and 1428 atomic, molecular, and predicted lines, respectively. In particular, by adapting also the log(gf) values of PLs, we minimized both the unavoidable underestimation of the blanketing in the synthetic spectra if PLs are ignored (see discussion in C14) and the risk of worsening the match with the observed spectrum if PLs with incorrect intensity are used (see Figure 3 in Munari et al. 2005). Therefore, on the basis of the above discussion, we confidently computed synthetic spectra for each of the ATLAS12 models listed in Section 2.1 and generated the final INTRIGOSS library.

The INTRIGOSS spectral library and the line list used to compute the synthetic spectra are available online together with auxiliary data as described in Section 4.

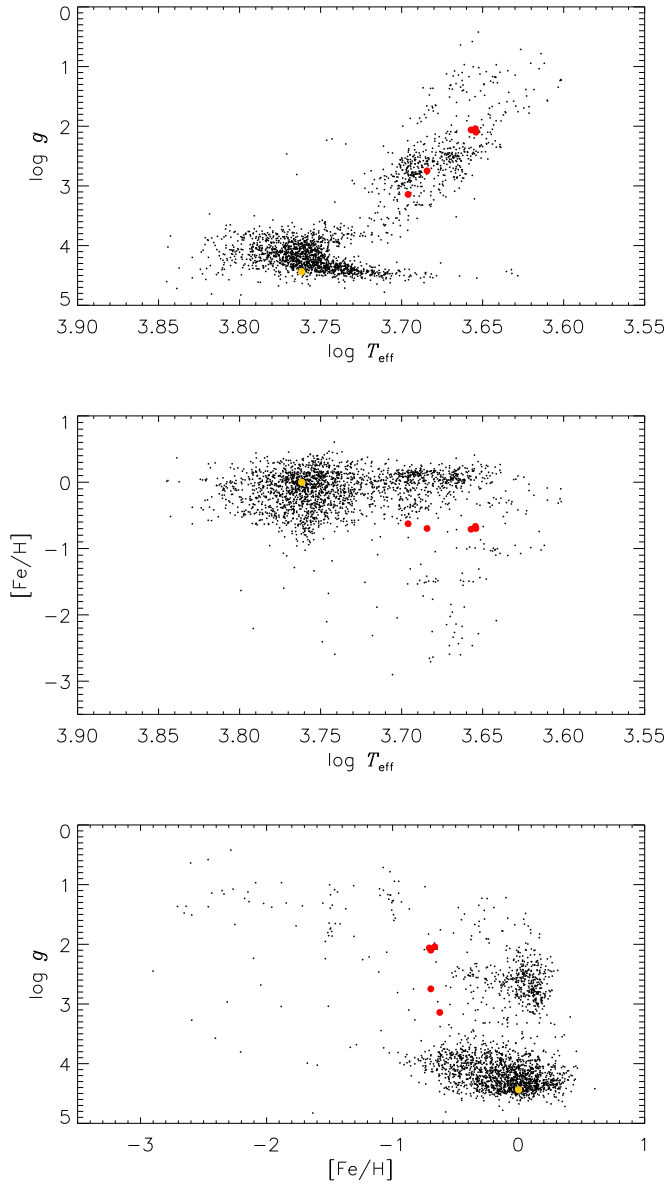

Figure 4. GES atmospheric parameters of the 2212 stars in the UVES-U580 sample (black points) with those of the Sun (yellow circle) and of the five giants in Table 1 (red circles) superimposed.

3. Comparison with Other Spectral Libraries

One of the main applications of stellar spectral libraries is the automatic analysis of spectra in stellar surveys to derive atmospheric parameters. Several examples can be found in the literature by using different spectral libraries and numerical codes, see for example García Pérez et al. (2016), Worley et al. (2016), B17, Kos et al. (2017), etc. The accuracy of the atmospheric parameters obtained depends both on the reliability of the input spectral libraries and on the algorithms implemented in the numerical codes used to derive them. It is therefore necessary to remove the effect of the different codes for estimating parameters if we want to compare the spectral libraries. Thus we decided to use as reference the UVES-U580 stars together with the homogeneously derived set of GES atmospheric parameter values that we consider as one of the best currently available. Therefore, the comparison of observed stellar spectra with the theoretical predictions of any synthetic stellar libraries can be safely performed by using these GES parameter values as input. In order to perform such a comparison we downloaded the following spectral libraries available online: AMBRE, GES_Grid,[25] PHOENIX, C14, and B17. To make a fair comparison, since we could not compute for each UVES-U580 star the corresponding *nominal* synthetic spectra from the literature libraries, we adopted the following approach: within the six (j) libraries and INTRIGOSS we computed the corresponding synthetic spectrum for each UVES-U580 star by linearly interpolating in $T_{\rm eff}$, $\log g$, [Fe/H], $\langle[\alpha/{\rm Fe}]\rangle$ or [Mg/Fe], and ξ at the *nominal* GES atmospheric parameter values. The interpolation procedure implies the addition of (systematic) errors that will depend on two main factors: the spacing in the grid nodes and the applied interpolation strategy (see for example Mészáros & Allende Prieto 2013). While a full analysis of the effects of interpolating within INTRIGOSS is beyond the scope of this paper, we hereafter provide some tests to estimate the errors associated with our linear interpolation.

In order to evaluate the errors introduced by our interpolation procedure we computed by using INTRIGOSS prescriptions the intra-mesh atmosphere models and the corresponding synthetic spectra, NSPs and FSPs, of 50 representative UVES-U580 stars, i.e., by using their nominal GES $T_{\rm eff}$, $\log g$, [Fe/H], $\langle[\alpha/{\rm Fe}]\rangle$, and ξ, but not their individual element abundances.[26] For each star we computed the mean value and the standard deviation ($\sigma_{\rm rd}$) of the relative differences between the interpolated and the intra-mesh spectra. The mean relative differences can be used to evaluate the interpolation error introduced in the overall spectrum levels while the standard deviations can be seen as an estimate of the "noise" introduced point-by-point. In the following Sections 3.1 and 3.2 we will use these values to provide estimates of the interpolation errors introduced by interpolating NSPs and FSPs, respectively.

3.1. The Normalized Synthetic Spectra, NSPs

We used the synthetic spectra obtained by interpolating the different j spectral libraries to normalize the corresponding UVES-U580 spectra and to compute the $r^j_{\rm med}$ figure of merit as described in Section 2.2. Due to the different wavelength and parameter space coverage of the six libraries, namely INTRIGOSS, AMBRE, GES_Grid, PHOENIX, C14, and B17, we restricted our analysis to their regions in common, i.e., 4900–5370 Å and $-1.0 \leqslant [{\rm Fe/H}] \leqslant 0.5$ dex, except for C14 which is limited to $[{\rm Fe/H}] \leqslant 0.2$ dex.

Figure 7 shows the trend of $\tilde{r}^j_{\rm med}$ for the different spectral libraries versus GES $T_{\rm eff}$, $\log g$, and [Fe/H]. Table 3 summarizes, for each spectral library j, the variations of $r^j_{\rm med}$ with respect to the *nominal* ones, as evaluated by computing $R^j_{\rm med} = {\rm median}\left(\frac{r^j_{\rm med}}{n\_r_{\rm med}}\right)$, i.e., the median value of the normalized $r_{\rm med}$s. As can be seen, the use of synthetic spectra computed at the $T_{\rm eff}$, $\log g$, [Fe/H], [Mg/Fe] or $\langle[\alpha/{\rm Fe}]\rangle$, and ξ by interpolating the INTRIGOSS library leads to a general increase of a few per cent in their $r_{\rm med}$s with respect to the corresponding $n_r_{\rm med}$s, thus confirming that the best agreement with the observed spectra can be reached, in general, by using

[25] It should be noticed that the GES_Grid library computed for internal GES use is based on the same methodology adopted when computing the AMBRE spectra (de Laverny et al. 2012) but with several improvements such as, in particular, a more accurate line list.

[26] These 50 intra-mesh synthetic spectra are also available on the website http://archives.ia2.inaf.it/intrigoss.

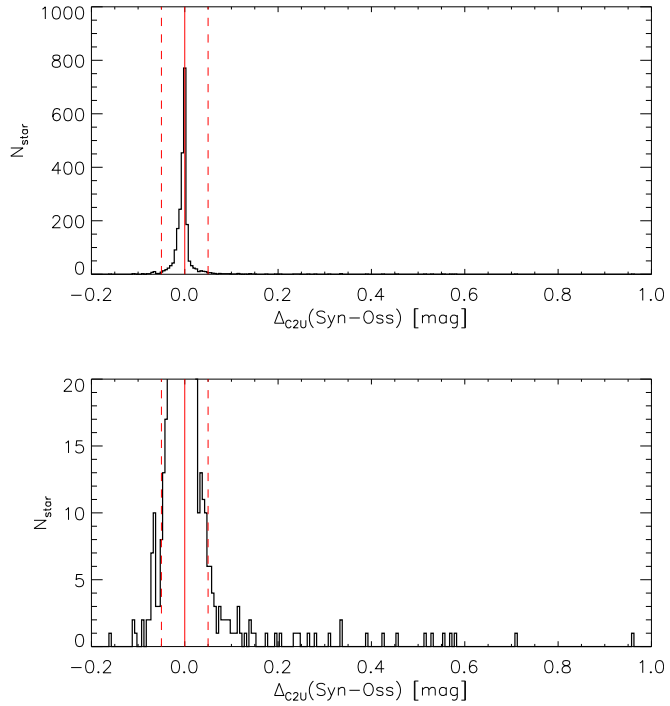

Figure 5. Distribution of the differences between C2U indices derived for each pair of synthetic and UVES-U580 spectra; the lower panel enlarges the *y*-scale and shows the presence of several outliers. Stars with $\Delta_{\rm C2U}$ values outside the red dashed lines (±0.05 mag) are removed from the UVES-U580 sample (see the text).

ad hoc models and the individual element abundances instead of the average metallicity and the average abundance ratio of the α-elements. Table 3 shows that slightly better results are obtained by interpolating according to the $\langle[\alpha/{\rm Fe}]\rangle$ stellar value instead of using [Mg/Fe], indicating that, even if one of the major contributors to absorption in this wavelength range is Mg (and MgH), the behavior of all the other α-elements also plays a non-negligible role and must be properly taken into consideration. The increase in $r_{\rm med}$s also contains the contribution introduced by the interpolation among the INTRIGOSS grid nodes. By comparing the 50 intra-mesh normalized synthetic spectra (see Section 3) with the corresponding interpolated ones, we found that the mean relative differences are of the order of ±0.1%, showing that the interpolation does not introduce significant inaccuracies in the overall normalized spectrum levels. As far as the relative standard deviations are concerned, the top panel of Figure 8 shows that $\sigma_{\rm rd}$ increases with decreasing temperature, showing that for $T_{\rm eff} \gtrsim 5500$ K interpolation errors become visible when working with spectra at S/N $\gtrsim$ 100 ($\sigma_{\rm rd} \simeq 0.01$), while for lower temperatures interpolation errors become significant also for S/N ∼ 50 ($\sigma_{\rm rd} \simeq 0.02$). Furthermore, from Figure 8 we can also see that for the other parameters, once the general trend of the standard deviations with $T_{\rm eff}$ is removed (linear fit shown in the first panel of Figure 8), the expected interpolation errors are less than 1% and do not show any significant trend with regard to the parameter values. On the basis of these results we plan to use a finer step in $T_{\rm eff}$ in the future extended version of INTRIGOSS in order to reduce interpolation errors.

As far as the other spectral libraries are concerned, we point out that the $\tilde{r}^{j}_{\rm med}$ in Figure 7 and the $R_{\rm med}$s in Table 3 obtained with the libraries AMBRE, GES_Grid, PHOENIX, C14, and B17 are much larger than those derived by using INTRIGOSS interpolated spectra (both INTRIGOSS$_{\rm Mg}$ and INTRIGOSS$_{\alpha}$). Their values include both the interpolation errors and the effects of the differences in physical assumptions and atomic and molecular line data in the different libraries. Unfortunately, the quantitative estimates of the uncertainties introduced by the interpolation cannot easily be given because we do not have at our disposal the equivalent intra-mesh synthetic spectra for AMBRE, GES_Grid, PHOENIX, C14, and B17. Furthermore, different libraries have different nodes, sometimes not equally spaced, and these differences may be reflected in different interpolation errors. Nevertheless, it is very unlikely that such large $R_{\rm med}$ values as those reported in Table 3 can be due only to the interpolation errors. Thus, we conclude that the differences in the $R_{\rm med}$ values indicate that INTRIGOSS spectra better reproduce the observed spectra of our UVES-U580 sample than the synthetic spectra from the other libraries.

The better performance of INTRIGOSS synthetic spectra can be inferred not only from the low $R_{\rm med}$ values in Table 3 but also from the much smaller spreads of their normalized $r_{\rm med}$ values, which reach a maximum of $\frac{r^{j}_{\rm med}}{n\_r_{\rm med}} = 1.6$ with only 10% of points above 1.2. On the other hand, not only are the $R_{\rm med}$ values for the other five libraries higher but also the spreads of the normalized $r^{j}_{\rm med}$s span an interval several units wide with 10% of the $\frac{r^{j}_{\rm med}}{n\_r_{\rm med}}$ values above 2.2, 1.9, 4.3, 2.6, and 2.2 for AMBRE, GES_Grid, PHOENIX, C14, and B17, respectively. In particular, inspection of Figure 7 shows that the coolest and/or most metal-rich stars are those characterized by higher $\tilde{r}^{j}_{\rm med}$ values, thus confirming that they are the most critical objects.

3.2. The Surface Flux Spectra, FSPs

3.2.1. Comparison of FSPs with Observed SEDs

In this section, the INTRIGOSS FSPs are compared with observed flux-calibrated spectra. A search for stars of our UVES-U580 sample within the ELODIE (Prugniel & Soubiran 2001; Prugniel et al. 2007), INDO–U.S. (Valdes et al. 2004), and MILES (Sánchez-Blázquez et al. 2006) SED libraries provided a list of about 20 stars in common. Eight of them are present in MILES and in at least one other SED library, and can be used to check the predictions of INTRIGOSS as far as the FSPs are concerned. We chose MILES as the reference SED source because it is one of the most used standard empirical libraries for stellar population models (see for example Vazdekis et al. 2015). Since only relative fluxes are needed, in general, for this kind of study we did not attempt to use absolute fluxes but we scaled the observed stellar SEDs and the corresponding synthetic spectra computed using the *nominal* GES atmospheric parameter values and the individual element abundances of each star (hereafter *n*_FSPs) according to their median flux value. In Figures 9 and 10 we plot the scaled *n*_FSPs and observed SEDs together with the residuals obtained after computing the average of the available SEDs, i.e., $\langle$SED$\rangle$-*n*_FSP, and the 3σ $\langle$SED$\rangle$ uncertainties. These two figures indicate that the *n*_FSPs for the stars at $T_{\rm eff} < 5300$ K reproduce, without any systematic trend, the mean observed SEDs within ∼3%, while for higher $T_{\rm eff}$ the agreement is within 1%. We also note, by looking at Figures 9 and 10, the absence of the excessive opacity near 5200 Å found by C14 in her synthetic spectra (see their Figure 10). We can conclude that the *n*_FSPs of the stars in Figures 9 and 10 accurately

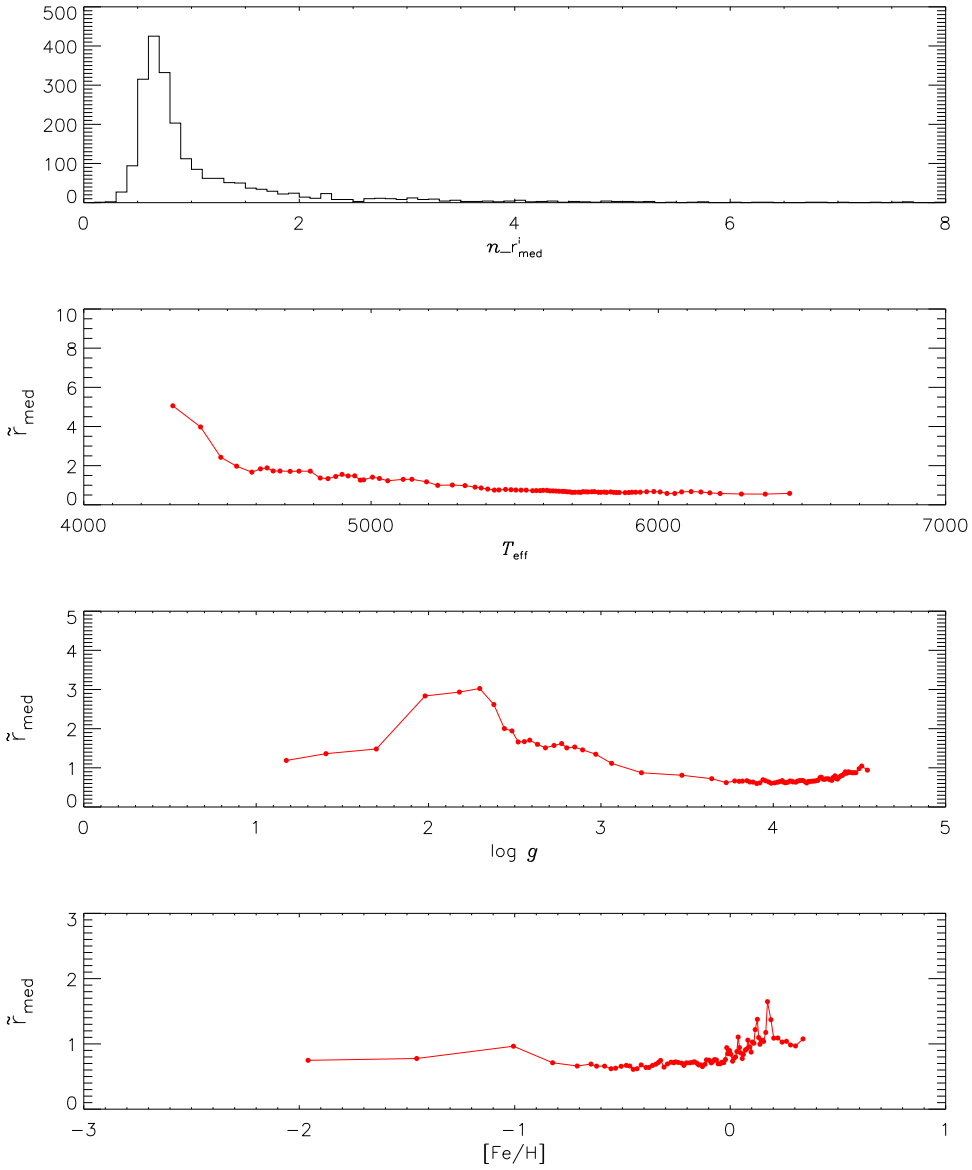

Figure 6. Distribution of $n\_r^i_{\rm med}$ obtained by using the *nominal* atmospheric parameter values in computing the synthetic spectra (top panel); the trend of the median values of $n\_r^i_{\rm med}$ computed in overlapped bins containing 51 stars each vs. $T_{\rm eff}$, log g, and [Fe/H] (second, third, and fourth panels respectively).

predict the observed SEDs. Unfortunately, the small number of UVES-U580 stars with accurate observed SEDs does not allow us to check in detail, through a complete coverage and a fine sampling, the accuracy of FPSs over the whole extent of the INTRIGOSS library in the atmospheric parameter space. Therefore, in the next section we will use, instead of SEDs, a different approach based on the comparison of spectral feature indices.

3.2.2. Comparison of Observed and Synthetic Mg_1, Mg_2, and Mgb Lick/SDSS indices

For a long time (and this is still the case), several spectroscopic analyses of stellar populations have relied on the Lick/IDS system of indices (Gorgas et al. 1993; Worthey et al. 1994, 2014; Worthey & Ottaviani 1997; Thomas et al. 2004; Korn et al. 2005). More recently, several authors have introduced new Lick-like systems (see for example Kim et al. 2016) to avoid the possible uncertainties associated with the response curve of the original Lick/IDS spectrograph and/or any potential loss of information that would occur in degrading spectra obtained from current surveys at medium resolution (e.g., $R \sim 1800$) such as the SDSS (York et al. 2000) or the Large Sky Area Multi-object Fiber Spectroscopic Telescope survey (LAMOST[27]) to match the low resolution ($R \sim 630$) of the original Lick/IDS system. One of these Lick-like systems is the Lick/SDSS (Franchini et al. 2010), which was built from observed energy distributions, SEDs, at $R = 1800$ and which is not affected by any particular instrumental signature. The Lick/SDSS indices are computed by integrating the spectrum in central bandpasses covering prominent stellar features after normalization to a pseudo-continuum defined via two bracketing blue and red side bands, and are therefore not very sensitive to small inaccuracies in the calibration of flux spectra. Nevertheless, since the three

[27] http://www.lamost.org/public/?locale=en

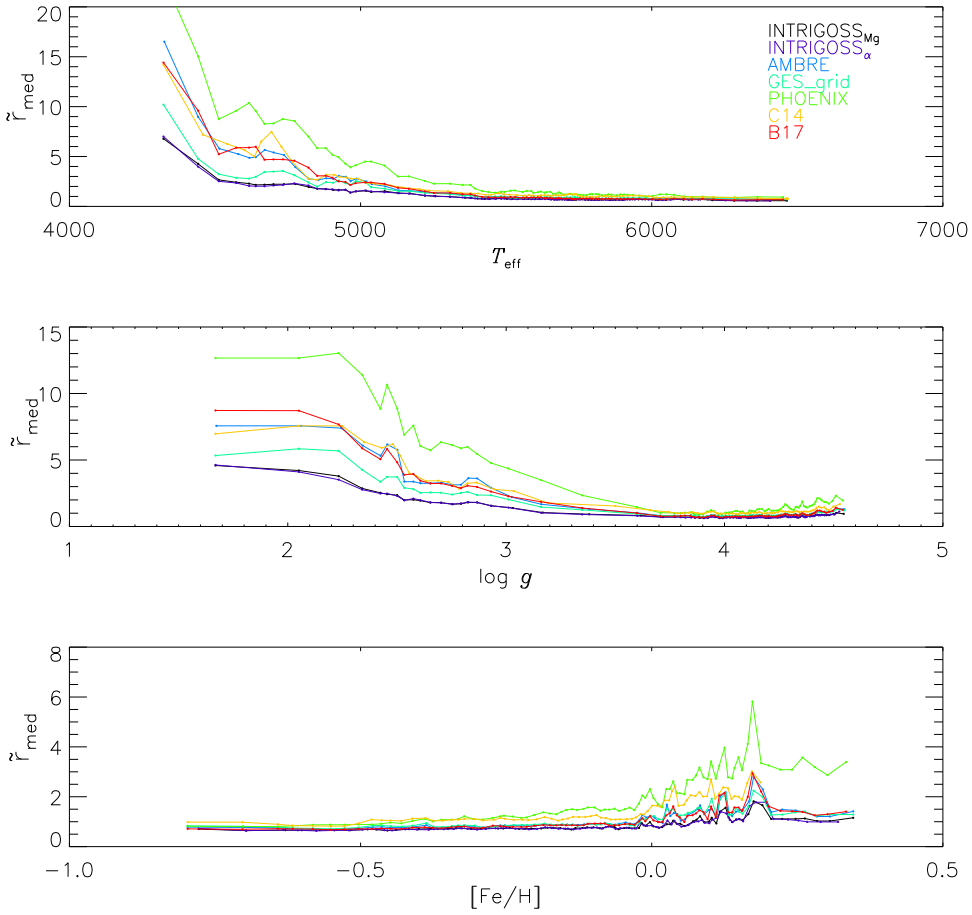

Figure 7. Trends of the median values of the computed r^{j}_{med}s for the different spectral libraries (identified by different colors) vs. GES T_{eff}, log g, and [Fe/H] (top to bottom); see the text and Figure 6.

bandpasses cover, in some cases, relatively large wavelength ranges, some indices are sensitive not only to the main absorption feature they were designed to measure, but also to the overall line blanketing present in the spectra. It is therefore possible to use them to check the accuracy and completeness of the atomic, molecular, and predicted lines used to compute the FSPs. In fact, if it turns out that the FSPs are able to accurately predict the observed indices, then the accuracy of the atomic and molecular absorption caused by the atmosphere models used to derive them, and therefore of the FSPs themselves, would be substantiated. In the following we will use the comparison between observational and synthetic Lick/SDSS indices as a method to evaluate the validity of the FSPs over the full atmospheric parameter space covered by the UVES-U580 stars. In particular, we chose the Mg_1, Mg_2, and Mgb indices, which are characterized by quite extended bandpasses falling in the wavelength region covered by our synthetic spectra. First we computed the observational indices, hereafter UVES-U580 indices, for each of the 2212 stars of the UVES-U580 sample, after removing the instrumental signature from the observed (stacked) UVES-U580 spectrum, degraded at $R = 1800$, by means of the corresponding *n*_FSP. Then, we computed the corresponding synthetic indices from INTRIGOSS FSPs and from the spectral libraries listed in Section 3.1 with the same interpolation adopted in Section 3.1. Unfortunately, the GES_Grid and B17 libraries contain only NSPs and cannot be used to compute Lick/SDSS indices. Therefore, we were able to compute the following synthetic indices:

1. *n*_FSP indices obtained from the above-defined *n*_FSPs;
2. *Interp*_FSP$_{\alpha}$ indices obtained from the spectra computed by interpolating INTRIGOSS FSPs at the stellar T_{eff}, log g, [Fe/H], ξ, and $\langle[\alpha/Fe]\rangle$;
3. *Interp*_FSP$_{Mg}$ indices obtained from the spectra computed by interpolating INTRIGOSS FSPs at the stellar [Mg/Fe] abundance ratio instead of at $\langle[\alpha/Fe]\rangle$;
4. *Interp*_PHOENIX indices obtained from the spectra computed by interpolating the flux-calibrated PHOENIX spectra at the stellar T_{eff}, log g, [Fe/H], and $\langle[\alpha/Fe]\rangle$;
5. *Interp*_C14 indices obtained from the spectra computed by interpolating the flux-calibrated C14 spectra at the stellar T_{eff}, log g, [Fe/H], and $\langle[\alpha/Fe]\rangle$.
6. *Interp*_AMBRE indices obtained from the spectra computed by interpolating the flux-calibrated AMBRE spectra at the stellar T_{eff}, log g, [Fe/H], and $\langle[\alpha/Fe]\rangle$.

While we were able to compute *n*_FSPs, and therefore the corresponding *n*_FSP indices, for all the stars in the UVES-U580 sample, the number of stars for which the interpolation within the spectral grids was possible varies because of the different parameter space coverages. In Figure 11 we plot the synthetic indices versus the UVES-U580 indices. Each panel contains the number of stars (N), the rms of the deviations from the 45° line, and the synthetic versus UVES-U580 regression lines. It can be seen that there is a very good agreement between *n*_FSP indices and UVES-U580 ones, indicating that the blanketing of the FSPs correctly predicts the observed

Table 3
Median Values of the Normalized r_{med}s for Different Spectral Libraries

Library	INTRIGOSS$_{Mg}$	INTRIGOSS$_{\alpha}$	AMBRE	GES_Grid	PHOENIX	C14	B17
R_{med}	1.043	1.025	1.313	1.266	2.161	1.700	1.298
σ	0.003	0.003	0.021	0.011	0.033	0.021	0.014

spectrum. The insignificant increase in the rms when using *Interp*_FSP$_{\alpha}$ and *Interp*_FSP$_{Mg}$ indices indicates that spectra computed from individual star models and element abundances provide synthetic indices that are almost equivalent to those obtained by *Interp*_FSPs. This result is different from that obtained by looking at the r_{med} values (see Section 3.1), and this could be ascribed to the sensitivity of the spectral index comparison being lower than that performed at each wavelength point.

The panels referring to *Interp*_PHOENIX, *Interp*_C14, and *Interp*_AMBRE indices show a larger rms and/or some systematic trend. The deviations of the Mg_1 and Mg_2 indices derived from PHOENIX and AMBRE spectra from the 45° line indicates significant differences in the blanketing predicted by these spectra. In the case of the indices derived from C14 spectra the deviations are smaller and the increase in rms is present only in Mg_2 and Mgb. It is worthwhile to recall that the comparison with the UVES-U580 indices is, in this case, limited to stars with $-1.0 < [Fe/H] < 0.2$ dex due to the absence of super-metal-rich spectra in the C14 library. The small systematic deviations may indicate that C14 has, on average, more accurate line lists than PHOENIX and that the increase in rms with respect to the upper panels may be due to the different treatment of the PLs.

Concerning the errors introduced by our interpolation procedure, we confirm the results already obtained in Section 3.1 also for FSPs. In addition, we computed intra-mesh FSPs for the seven stars in Figures 9 and 10 for which we were able to compute interpolated INTRIGOSS FSPs.[28] Then, we compare the 3σ uncertainties of the $\langle SED \rangle$ of these stars with the differences between the intra-mesh and the interpolated INTRIGOSS FSPs. Figure 12 shows that the interpolation procedure introduces inaccuracies in the spectra (red lines) that are well below the uncertainties of the SEDs (yellow areas).

Eventually, we compared the *Interp*_FSP$_{\alpha}$ indices with those computed by using the 50 intra-mesh FSPs to estimate the effect of the interpolation on the computation of the indices, and we did not find any systematic trend in the differences. The use of the interpolated spectra instead of the intra-mesh ones introduces an rms scatter that is one order of magnitude smaller than those reported in the first row of Figure 11, showing that the interpolation error on the indices does not undermine the above-given discussion about the indices computed with the different spectral libraries.

In conclusion, the comparison of observational and synthetic Mg_1, Mg_2, and Mgb Lick/SDSS indices indicates that the INTRIGOSS FSPs predict the observed blanketing well, thus suggesting that this library can provide accurate synthetic SEDs not only for the stars discussed in Section 3.2.1 but also for all of those in the UVES-U580 sample.

[28] We cannot compute the interpolated synthetic spectrum for the UVES-U580 star 09485645+1344286 (HD 084937) since its [Fe/H] is −2.21 dex.

4. Data Products

The INTRIGOSS spectral library and the line list used to compute the synthetic spectra are available on the website http://archives.ia2.inaf.it/intrigoss together with auxiliary data.

The synthetic spectra are computed from 4830 to 5400 Å at wavelength sampling $\Delta\lambda = 0.01$ Å, rotational velocity of $0\,km\,s^{-1}$, and, in order to be consistent with the ATLAS12 models, with microturbulent velocities $\xi = 1$ and $2\,km\,s^{-1}$, leading to a final total number of 7616 NSPs and 7616 FSPs.

The gaps in the final grid are due to the absence of converging ATLAS12 atmosphere models for $\log g = 0.5$ dex and $T_{eff} \geqslant 6250$ K. In order to keep the grid homogeneous, we decided to avoid any patches based on, for example, the use of ATLAS9 atmosphere models. Work is in progress to attain convergence of ATLAS12 code at relatively high temperatures and low surface gravities.

The INTRIGOSS spectra are provided in FITS binary table format and can be downloaded by selecting:

1. the type of spectra: NSP, FSP, or both;
2. a range in T_{eff} and/or $\log g$ and/or [Fe/H] and/or [α/Fe] and/or ξ, or the whole library (15,232 spectra);

The following auxiliary data are also available from links given in the http://archives.ia2.inaf.it/intrigoss-details webpage:

1. A FITS binary table with the line list of atomic and molecular transitions used in computing INTRIGOSS synthetic spectra. The table contains 1427,628 entries in the format of the line list file used by SPECTRUM code (see Section 3.3.1 and 3.6 of Documentation for SPECTRUM, Gray & Corbally 1994), i.e., for each line we list:
   WAVELENGTH: wavelength in Å;
   ELEM_ION: element and ion identifier, e.g., 26.1 for Fe II;
   ISOTOPE: mass number of isotope (the 0 code corresponds to entries representing all possible isotopes for that species taken together);
   ELOW: energy of the lower state in cm^{-1};
   EHIGH: energy of the upper state in cm^{-1}; this entry is sometimes used to encode the molecular band information since only ELOW is used in molecular calculation;
   LOG_GF: the logarithm of the product of the statistical weight of the lower level and the oscillator strength for the transition;
   FUDGE: a fudge factor to adjust the line broadening;
   TRANSITION_TYPE: the type of transition;
   REFERENCE: The subset of lines with derived astrophysical *gf*-values are indicated as FRA18 and FRA18_P for laboratory and predicted lines, respectively.
2. A FITS binary image with the solar spectrum observed with very high S/N (∼4000) described in Section 2.2.1 and used to derive astrophysical $\log(gf)$ values.
3. A set of 100 FITS binary tables with synthetic spectra (50 NSPs and 50 FSPs) computed at 50 representative intra-

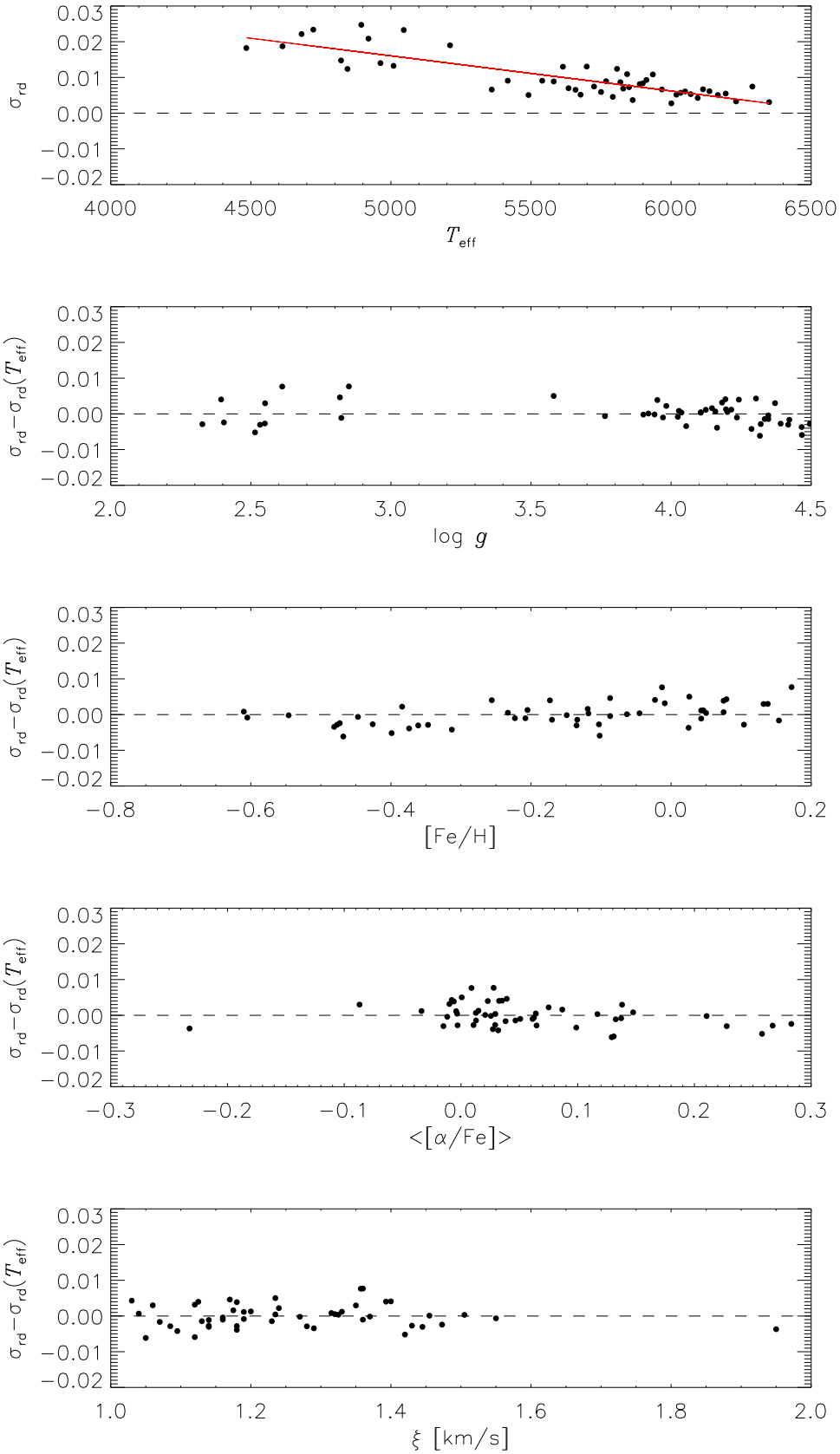

Figure 8. Trends of the standard deviation (σ_{rd}) of the relative differences between the 50 interpolated and intra-mesh NSPs vs. T_{eff}, log g, [Fe/H], $\langle[\alpha/Fe]\rangle$, and ξ. The general trend of σ_{rd} vs. T_{eff}, $\sigma_{rd}(T_{eff})$, as derived by a linear regression (red line in the top panel), has been subtracted from σ_{rd} in the other panels.

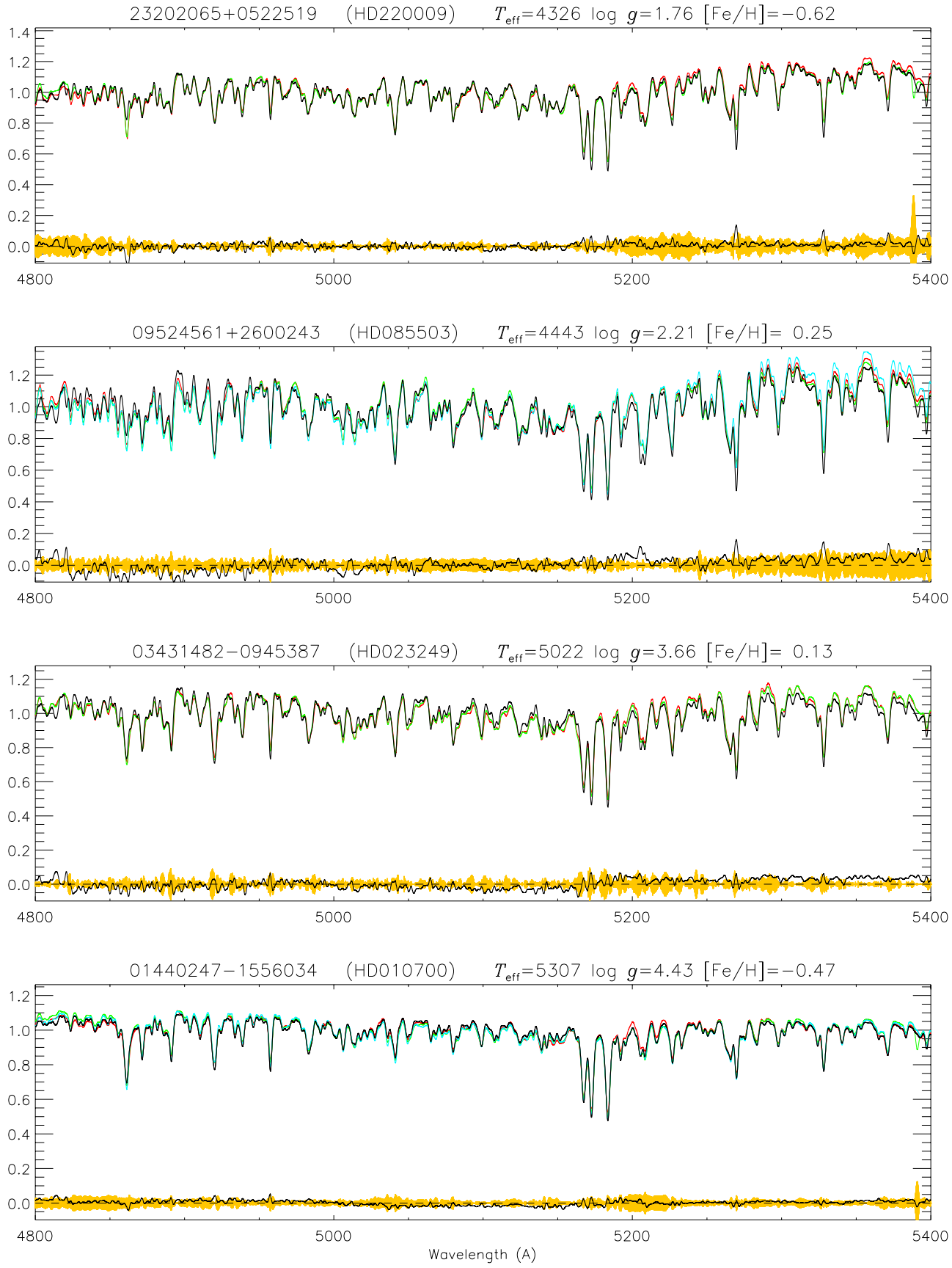

Figure 9. Comparison of flux-calibrated spectra (MILES in red, Indo–US in green, and ELODIE in light blue) scaled according to their median values and the corresponding *n*_FSPs (black). The black curve at the bottom of each panel shows the flux difference, i.e., the average of the observations minus the corresponding *n*_FSP, superimposed on the 3σ of the observed spectra (yellow area).

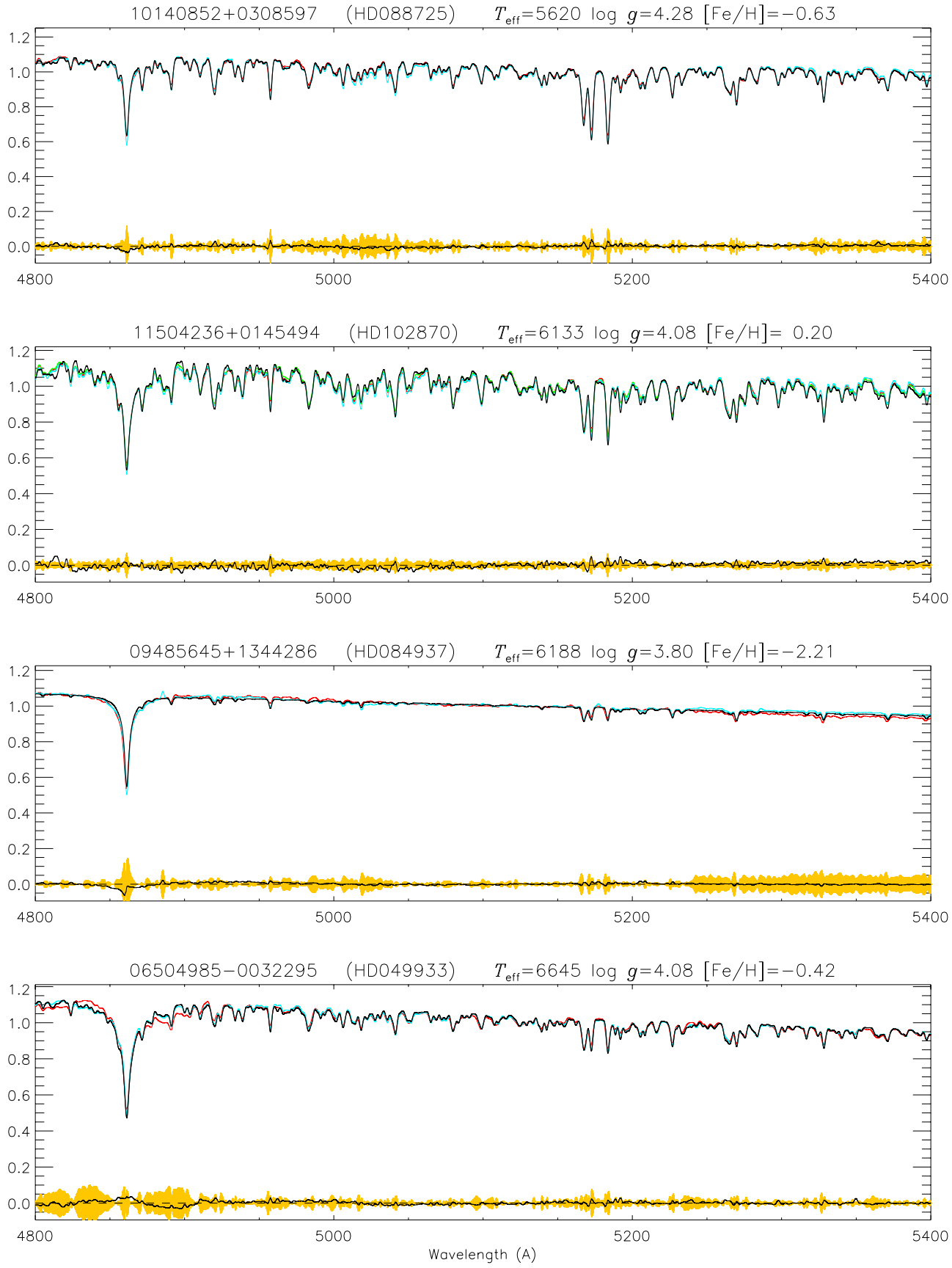

Figure 10. As in Figure 9.

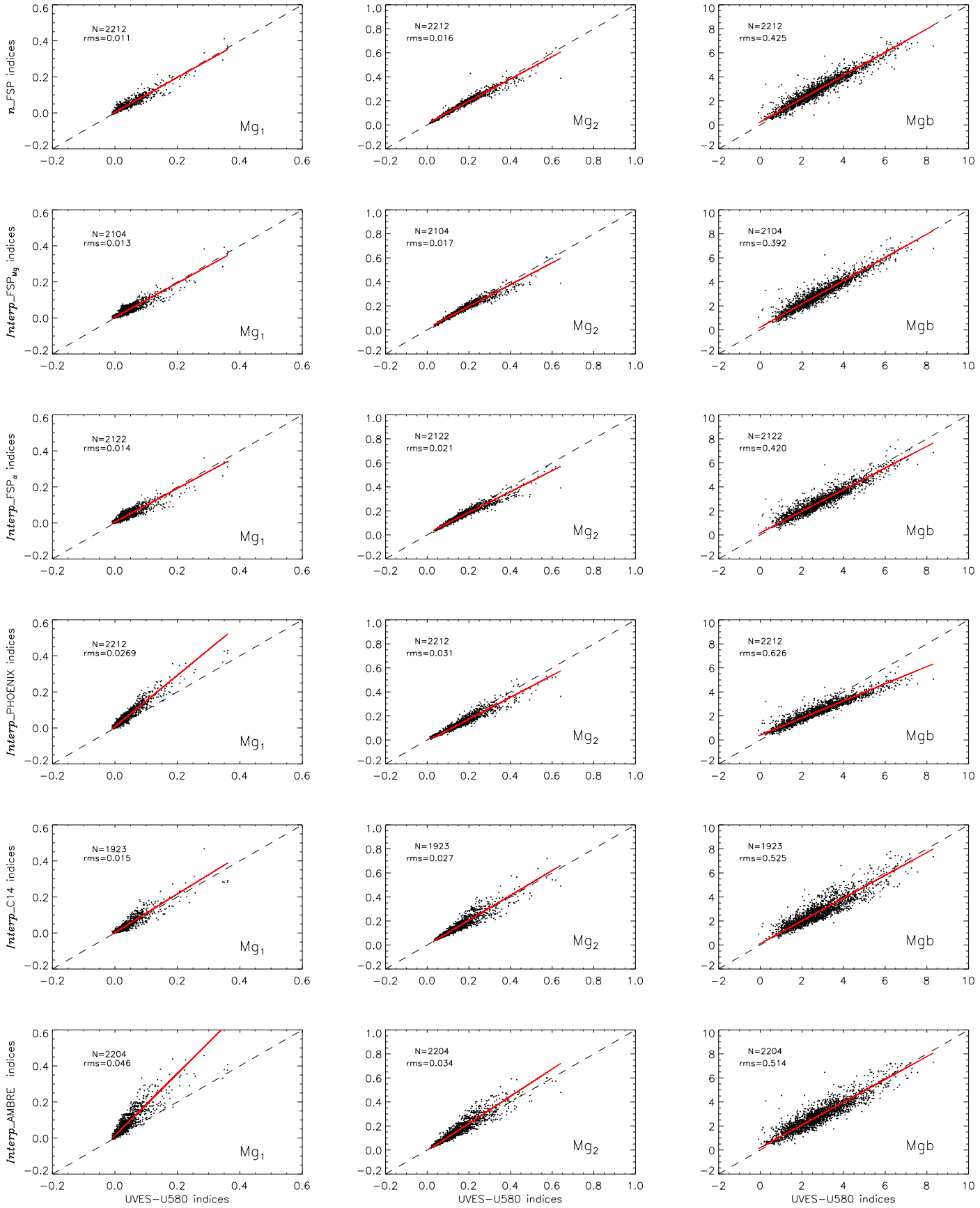

Figure 11. Comparison of synthetic and observational Lick/SDSS indices Mg_1 (left panels), Mg_2 (central panels), and Mgb (right panels). Indices computed from synthetic spectra are plotted vs. those measured from UVES-U580 spectra (see the text) together with the 45° (dashed) and the regression (red) lines. From top to bottom: *n*_FSP indices computed from *n*_FSPs; *Interp*_FSP$_{Mg}$ and *Interp*_FSP$_{\alpha}$ indices computed from INTRIGOSS; *Interp*_PHOENIX, *Interp*_C14, and *Interp*_AMBRE indices computed from PHOENIX, C14, and AMBRE libraries respectively (see the text).

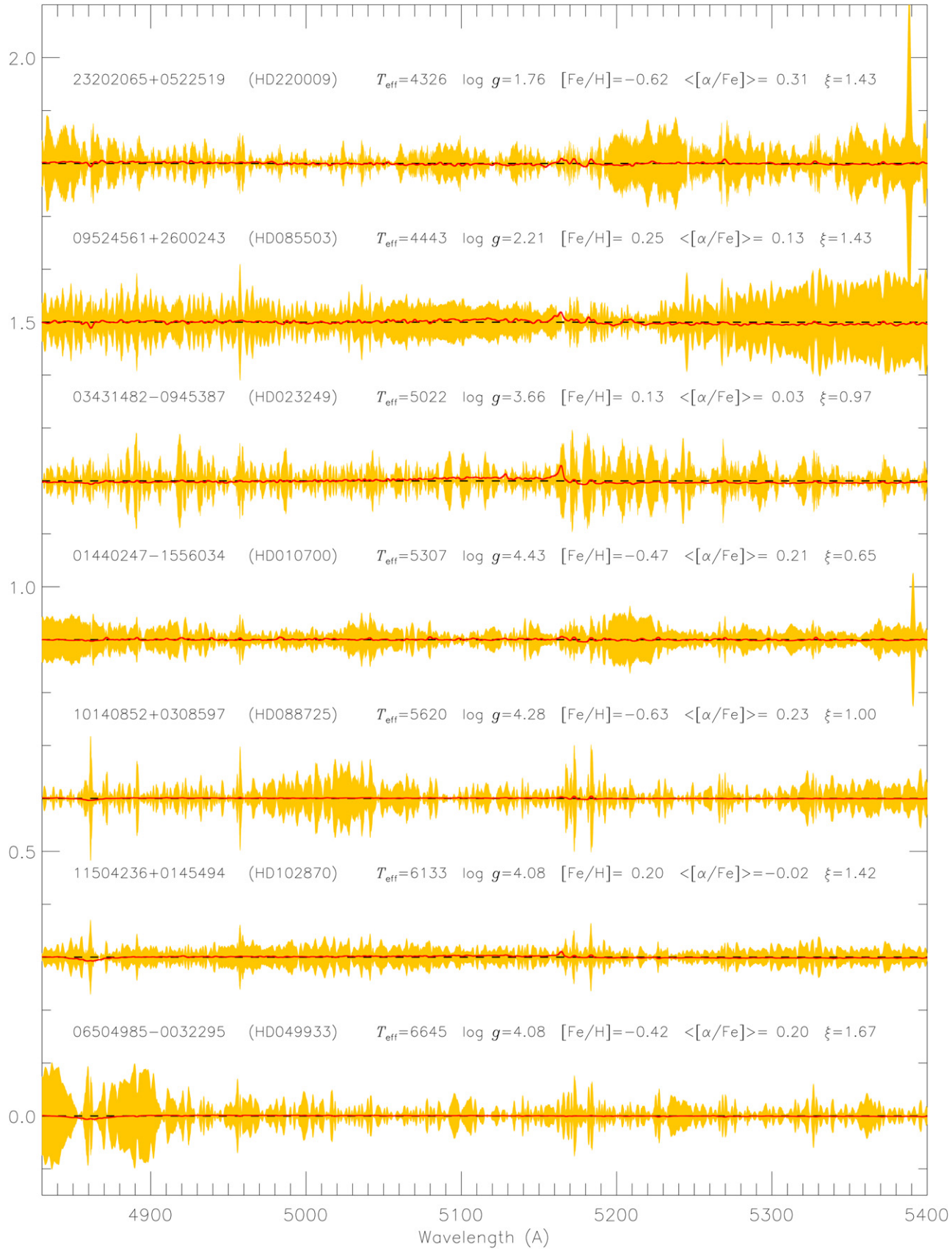

Figure 12. Comparison between the 3σ of the ⟨SEDs⟩ (yellow area) and the differences between the intra-mesh and the interpolated INTRIGOSS FSPs (red lines) for seven of the stars discussed in Section 3.2. Horizontal dashed black lines represent the zero levels after vertical shifts applied to better visualize all the stars in the same plot.

Table 4
Unidentified Spectral Lines

	Sun	00241708–7206106	00251219–7208053	00240054–7208550	02561410–0029286	03173493–0022132
σ	0.03	0.04	0.04	0.04	0.03	0.03
Wavelength (Å)	Depth	Depth	Depth	Depth	Depth	Depth
4834.60	0.08	0.12	0.04	0.10	0.05	…
4844.19	…	…	…	**0.14**	…	…
4855.20	0.05	…	**0.17**	…	…	…
4858.14	**0.11**	…	0.08	…	0.06	…
4861.95	0.08	**0.20**	**0.21**	**0.18**	**0.15**	**0.11**
4866.72	0.04	…	…	…	…	**0.09**
4880.97	0.06	0.08	…	0.09	0.07	0.04
4884.94	**0.13**	**0.16**	**0.21**	**0.15**	**0.11**	**0.10**
4906.80	0.07	…	0.08	0.05	…	0.03
4916.23	0.07	0.03	0.06	0.03	…	…
4916.49	**0.14**	0.04	0.10	0.06	…	…
4921.85	…	…	…	…	…	**0.14**
4922.81	0.07	…	…	…	…	…
4927.88	**0.59**	**0.40**	**0.43**	**0.42**	**0.33**	**0.35**
4934.20	…	…	…	**0.22**	…	…
4937.09	0.07	…	…	…	…	…
4940.06	**0.16**	0.10	0.10	0.09	0.04	0.06
4940.50	0.08	…	…	…	…	…
4944.29	**0.11**	…	…	…	…	0.03
4948.33	0.07	…	0.09	…	…	…
4954.60	…	…	…	…	…	**0.10**
4961.05	**0.13**	0.10	**0.15**	0.10	0.07	0.07
4964.14	0.08	…	…	…	…	…
4966.29	0.09	0.09	0.11	0.08	0.08	0.04
4971.35	**0.51**	**0.29**	**0.31**	**0.32**	**0.27**	**0.30**
4990.45	**0.27**	**0.18**	**0.22**	**0.19**	**0.16**	**0.13**
5013.93	**0.17**	**0.13**	0.09	0.11	0.08	0.08
5016.89	**0.44**	**0.28**	**0.27**	**0.27**	**0.22**	**0.22**
5031.18	0.06	…	0.07	0.06	…	…
5036.28	**0.43**	**0.30**	**0.31**	**0.29**	**0.22**	**0.22**
5041.34	0.07	0.09	0.07	0.06	0.05	0.07
5041.44	0.08	0.11	0.09	0.09	0.05	0.07
5088.16	**0.18**	0.10	0.11	0.10	0.06	**0.09**
5092.29	0.07	…	0.04	0.04	0.04	0.05
5097.49	**0.38**	**0.24**	**0.24**	**0.23**	**0.19**	**0.18**
5136.27	0.08	0.05	0.08	…	…	…
5140.82	**0.14**	0.08	0.09	0.09	0.04	0.05
5156.66	**0.13**	…	0.06	0.06	0.05	0.07
5157.21	0.08	…	…	…	…	…
5169.30	**0.14**	0.08	0.08	0.08	0.07	0.06
5170.77	**0.29**	0.10	0.10	0.10	0.09	0.08
5179.78	0.03	…	…	…	…	**0.10**
5181.32	**0.16**	…	…	…	…	…
5212.22	0.08	…	0.06	…	…	…
5214.61	**0.11**	0.05	0.03	0.04	0.05	0.03
5215.57	**0.14**	…	…	…	…	…
5217.89	**0.13**	…	…	…	…	…
5221.03	**0.20**	0.12	0.12	0.09	0.09	**0.10**
5221.75	**0.12**	0.04	…	0.06	…	0.03
5225.81	**0.14**	…	…	…	…	…
5226.13	0.08	0.05	0.02	0.04	0.03	…
5228.10	**0.12**	…	…	…	…	…
5242.06	**0.15**	0.06	…	…	…	0.06
5243.18	**0.10**	0.06	…	…	…	0.03
5248.98	0.08	0.09	0.10	0.08	0.07	0.05
5255.70	0.07	0.08	0.10	0.12	0.05	0.06
5263.77	0.07	0.09	…	…	…	…
5272.00	0.09	…	…	…	…	…
5274.53	**0.10**	0.06	0.05	0.06	…	0.04
5275.13	**0.22**	…	…	…	…	…
5276.17	0.07	…	0.08	0.08	…	0.06
5278.78	0.08	…	…	…	…	…

Table 4
(Continued)

	Sun	00241708–7206106	00251219–7208053	00240054–7208550	02561410–0029286	03173493–0022132
σ	0.03	0.04	0.04	0.04	0.03	0.03
5281.32	**0.10**	⋯	⋯	⋯	⋯	⋯
5284.34	⋯	⋯	**0.21**	**0.16**	⋯	⋯
5298.51	**0.11**	⋯	⋯	⋯	⋯	⋯
5299.97	**0.11**	⋯	⋯	⋯	⋯	⋯
5303.84	0.06	⋯	⋯	⋯	⋯	⋯
5314.92	0.07	⋯	⋯	0.03	⋯	⋯
5341.15	**0.27**	**0.30**	**0.25**	**0.29**	**0.23**	**0.22**
5370.30	0.06	0.04	0.06	⋯	⋯	0.04
5389.85	0.09	⋯	0.08	⋯	⋯	⋯
5390.53	**0.19**	⋯	0.05	0.05	0.04	0.06

Note. Depth values larger than 3σ are in bold.

mesh positions. These spectra are used in Section 3.1 to test the errors arising from our interpolation procedure of the INTRIGOSS spectra.

5. Summary

In this paper we present a new high-resolution synthetic spectral library, INTRIGOSS, which covers the parameter space range of F, G, and K stars. INTRIGOSS is based on atmosphere models computed with ATLAS12, which allowed us to specify each individual element abundance. The normalized spectra (NSPs) and surface flux spectra (FSPs), in the wavelength range 4830–5400 Å, were computed in a fully consistent mode by means of SPECTRUM v2.76f code using the detailed solar composition of Grevesse et al. (2007) and varying it by adopting different [α/Fe] abundance ratios. Particular attention was devoted to deriving astrophysical *gf*-values by comparing synthetic predictions with a solar spectrum of very high S/N and UVES-U580 spectra of cool giants with good S/N. The validity of the obtained spectra, and in particular of the astrophysical *gf*-values used, was assessed by using as reference more than 2000 stars with homogeneously and accurately derived atmospheric parameter values and detailed chemical compositions.

The greater accuracy of INTRIGOSS NSPs with respect to other publicly available stellar libraries, i.e., AMBRE, GES_Grid, PHOENIX, C14, and B17, in reproducing the observed spectra was shown by computing a figure of merit, $r_{\rm med}$, to evaluate the consistency of the prediction of different libraries with respect to the spectra of the stars in the UVES-U580 sample.

As far as the FSPs are concerned, the comparison with SEDs derived from ELODIE, INDO–U.S., and MILES libraries showed that they reproduce the observed flux distributions within a few per cent without any systematic trend. A check on the predicted blanketing of FSPs, and therefore on the adopted line lists (including the treatment of the PLs) based on comparison of Lick/SDSS indices confirmed the reliability of INTRIGOSS surface flux spectra and their ability to reproduce the observational index values better than PHOENIX, AMBRE, and C14 libraries.

The results of the validity checks on both INTRIGOSS normalized spectra (NSPs) and surface flux spectra (FSPs) make us confident that the presented spectral library, which is available on the web together with the adopted line list and the observed solar spectrum (see Section 4), will provide to the astronomical community a valuable tool both for determinations of stellar atmospheric parameters and for stellar population studies.

This work is based on data products from observations made with ESO Telescopes at the La Silla Paranal Observatory under programme ID 188.B-3002. These data products have been processed by the Cambridge Astronomy Survey Unit (CASU) at the Institute of Astronomy, University of Cambridge, and by the FLAMES/UVES reduction team at INAF/Osservatorio Astrofisico di Arcetri. These data have been obtained from the *Gaia*–ESO Survey Data Archive, prepared and hosted by the Wide Field Astronomy Unit, Institute for Astronomy, University of Edinburgh, which is funded by the UK Science and Technology Facilities Council. This work was partly supported by the European Union FP7 programme through ERC grant number 320360 and by the Leverhulme Trust through grant RPG-2012-541. We acknowledge the support from INAF and Ministero dell' Istruzione, dell' Università e della Ricerca (MIUR) in the form of the grant "Premiale VLT 2012." The results presented here benefit from discussions held during the *Gaia*–ESO workshops and conferences supported by the ESF (European Science Foundation) through the GREAT Research Network Programme. This work received partial financial support from PRIN MIUR 2010–2011 project "The Chemical and Dynamical Evolution of the Milky Way and Local Group Galaxies," prot. 2010LY5N2T and by the National Institute for Astrophysics (INAF) through the grant PRIN-2014 ("The *Gaia*–ESO Survey"). M.C. thanks financial support from CONACyT grant CB-2015-256961. This research uses the facilities of the Italian Center for Astronomical Archive (IA2) operated by INAF.

Facility: VLT:Kueyen.

Software: SPECTRUM (v2.76f; Gray & Corbally 1994), ATLAS12 (Kurucz 2005a), LineSearcher (Sousa et al. 2015).

Appendix
Unidentified Spectral Features

Together with the accurate determination of astrophysical log(*gf*) values, the analysis of the solar spectrum and of the GES spectra of the five giant stars in Table 1 allows us to determine where the adopted line list is missing features. To construct the list of these unidentified features we computed the difference between the observed and synthetic spectra of the Sun and of the five giants and the corresponding standard

Table 5
Number of Unidentified Features

Star	N_{tot}	$N_{2\sigma-3\sigma}$	$N_{>3\sigma}$
Sun	67	25	35
00241708–7206106	36	11	10
00251219–7208053	42	12	12
00240054–7208550	40	11	12
02561410–0029286	30	8	9
03173493–0022132	39	10	17

deviations (σ_{Sun}, σ_i). Then, we ran the *LineSearcher* code, which is a derivation from the ARES code (Sousa et al. 2015), using as input the six files of the differences and we obtained for all the *absorption features* in the differences, i.e., those below zero, their central wavelength and depth. Eventually, we extracted from the solar *LineSearcher* output all the features that have a depth larger than $2\sigma_{Sun}$, while a $3\sigma_i$ threshold was used in the case of the five giants, due to the lower resolution and S/N of their spectra. At the end we checked whether the features thus selected were present in more than one spectrum but with smaller depths. Table 4 lists the wavelength of each unidentified feature together with its depth in all the stars in which it is detectable, while Table 5 shows the total number of detected unidentified features in each stellar spectrum (column 2), and the numbers of those with depth between 2σ and 3σ (column 3) and larger than 3σ (column 4).

ORCID iDs

Mariagrazia Franchini https://orcid.org/0000-0001-5611-2333
Ettore Flaccomio https://orcid.org/0000-0002-3638-5788
Sergey E. Koposov https://orcid.org/0000-0003-2644-135X
Amelia Bayo https://orcid.org/0000-0001-7868-7031
Giovanni Carraro https://orcid.org/0000-0002-0155-9434
Andy Casey https://orcid.org/0000-0003-0174-0564
Carmela Lardo https://orcid.org/0000-0002-4295-8773
Tomaz Zwitter https://orcid.org/0000-0002-2325-8763

References

Anders, E., & Grevesse, N. 1989, GeCoA, 53, 197
Brahm, R., Jordán, A., Hartman, J., & Bakos, G. 2017, MNRAS, 467, 971, (B17)
Castelli, F. 2005, MSAIS, 8, 34
Castelli, F., & Kurucz, R. L. 2003, in IAU Symp. 210, Modelling of Stellar Atmosphere, ed. N. E. Piskunov, W. W. Weiss, & D. F. Gray (San Francisco, CA: ASP), A20
Coelho, P., Barbuy, B., Meléndez, J., et al. 2005, A&A, 443, 735
Coelho, P. R. T. 2014, MNRAS, 440, 1027
Dekker, H., D'Odorico, S., Kaufer, A., Delabre, B., & Kotzlowski, H. 2000, Proc. SPIE, 4008, 534
de Laverny, P., Recio-Blanco, A., Worley, C. C., & Plez, B. 2012, A&A, 544, A126
De Silva, G. M., Freeman, K. C., Bland-Hawthorn, J., et al. 2015, MNRAS, 449, 2604
Franchini, M., Morossi, C., Di Marcantonio, P., Malagnini, M. L., & Chavez, M. 2010, ApJ, 719, 240
García Pérez, A. E., Allende Prieto, C., Holtzman, J. A., et al. 2016, AJ, 151, 144
Gilmore, G., Randich, S., Asplund, M., et al. 2012, Msngr, 147, 25
Gonneau, A., Lancon, A., Trager, S. C., et al. 2016, A&A, 589, A36
Gorgas, J., Faber, S. M., Burstein, D., et al. 1993, ApJS, 86, 153
Gray, R. O., & Corbally, D. J. L. I. 1994, AJ, 107, 742
Grevesse, N., Asplund, M., & Sauval, A. J. 2007, SSRv, 130, 105
Gustafsson, B., Edvardsson, B., Eriksson, K., et al. 2008, A&A, 486, 951
Hauschildt, P. H., & Baron, E. 1999, JCoAM, 109, 41
Hubeny, I. 1988, CoPhC, 52, 103
Husser, T.-O., Wende-von Berg, S., Dreizler, S., et al. 2013, A&A, 553, A6
Jacoby, G. H., Hunter, D. A., & Christian, C. A. 1984, ApJS, 56, 257
Jofré, P., Heiter, U., Soubiran, C., et al. 2015, A&A, 582, A81
Kim, H.-S, Cho, J., Sharpless, R. M., et al. 2016, ApJS, 227, 24
Korn, A., Maraston, C., & Thomas, D. 2005, A&A, 438, 685
Kos, J., Lin, J., Zwitter, T., et al. 2017, MNRAS, 464, 1259
Kurucz, R. L. 1979, ApJS, 40, 1
Kurucz, R. L. 2005a, MSAIS, 8, 14
Kurucz, R. L. 2005b, MSAIS, 8, 76
Kurucz, R. L. 2014, in Determination of Atmospheric Parameters of B-, A-, F- and G-Type Stars, ed. E. Niemczura, B. Smalley, & W. Pych (Cham: Springer), 63
Leitherer, C., Alloin, D., Alvensleben, U. F.-v., et al. 1996, PASP, 108, 996
Lobel, A. 2011, CaJPh, 89, 395
Magrini, L., Randich, S., Kordopatis, G., et al. 2017, A&A, 603A, 2
Majewski, S. R., Schiavon, R. P., Frinchaboy, P. M., et al. 2017, AJ, 154, 94
Mészáros, Sz., & Allende Prieto, C. 2013, MNRAS, 430, 3285
Molaro, P., Monaco, L., Barbieri, M., & Zaggia, S. 2013, MNRAS, 429, 79
Moultaka, J., Ilovaisky, S. A., Prugniel, P., & Soubiran, C. 2004, PASP, 116, 693
Munari, U., Sordo, R., Castelli, F., & Zwitter, T. 2005, A&A, 442, 1127
Partridge, H., & Schwenke, D. W. 1997, JChPh, 106, 4618
Prugniel, Ph., & Soubiran, C. 2001, A&A, 369, 1048
Prugniel, Ph., et al. 2007, arXiv:astro-ph/0703658
Randich, S., Gilmore, G. & Gaia–ESO Consortium 2013, Msngr, 154, 47
Sacco, G. G., Morbidelli, L., Franciosini, E., et al. 2014, A&A, 565, 513
Sánchez-Blázquez, P., Peletier, R. F., Jimenez-Vicente, J., et al. 2006, MNRAS, 371, 703
Schwenke, D. W. 1998, FaDi, 109, 321
Smiljanic, R., Korn, A. J., Bergemann, M., et al. 2014, A&A, 570, A122
Sousa, S. G., Santos, N. C., Adibekyan, V., Delgado-Mena, E., & Israelian, G. 2015, A&A, 577, A67
Swan, W. 1857, Transactions of the Royal Society of Edinburgh, 21, 411
Thomas, D., Maraston, C., & Korn, A. 2004, MNRAS, 351, L19
Valdes, F., Gupta, R., Rose, J. A., Singh, H. P., & Bell, D. J. 2004, ApJS, 152, 251
Vazdekis, A., Coelho, P., Cassisi, S., et al. 2015, MNRAS, 449, 1177
Weck, P. F., Schweitzer, A., Stancil, P. C., Hauschildt, P. H., & Kirby, K. 2003, ApJ, 582, 1059
Worley, C. C., de Laverny, P., Recio-Blanco, A., Hill, V., & Bijaoui, A. 2016, A&A, 591, A81
Worthey, G., Danilet, A. B., & Faber, S. M. 2014, A&A, 561, A36
Worthey, G., Faber, S. M., Gonzalez, J. J., & Burstein, D. 1994, ApJS, 94, 687
Worthey, G., & Ottaviani, D. L. 1997, ApJS, 111, 377
Yanny, B., Rockosi, C., Newberg, H. J., et al. 2009, AJ, 137, 4377
York, D. G., Adelman, J., Anderson, J. E., et al. 2000, AJ, 120, 1579